



## Review

# Micro-Nano Bubbles Coupled with Ozone Catalyzed Oxidation for the Treatment of Organic Wastewater: A Review

Xiao Wang<sup>1</sup>, Jie Yu<sup>1\*</sup>, Cong Geng<sup>1</sup>, Jie Zhang<sup>1</sup>, Zi-Ang Wang<sup>1</sup>, Meng Zhu<sup>1</sup>, Mingyuan Ye<sup>1</sup>, Yuhan Wu<sup>1,2</sup>

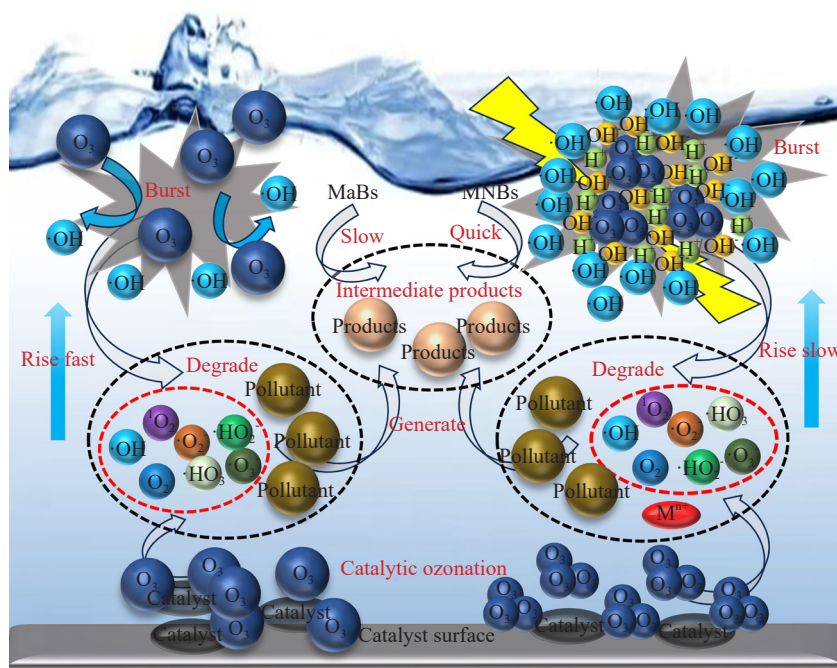
<sup>1</sup>School of Environmental and Chemical Engineering, Shenyang University of Technology, Shenyang, 110870, China

<sup>2</sup>School of Chemistry and Chemical Engineering, State Key Laboratory Incubation Base for Green Processing of Chemical Engineering, Shihezi, 32003, China

E-mail: [jieyu@sut.edu.cn](mailto:jieyu@sut.edu.cn)

Received: 6 December 2024; Revised: 4 March 2025; Accepted: 10 March 2025

### Graphical Abstract:



As shown in the left part of the figure, traditional ozone macrobubbles ( $O_3$ /MaBs) combined with ozone catalytic oxidation technology effectively degrade pollutants. The right part of the figure illustrates ozone micro-nano bubbles ( $O_3$ /MNBs) used in conjunction with ozone catalytic oxidation. The smaller diameter of ozone nanobubbles rises more slowly than larger ozone bubbles, which increases their residence time in solution. The high temperature and pressure,

Copyright ©2025 Jie Yu, et al.

DOI: <https://doi.org/10.37256/fce.6120256217>

This is an open-access article distributed under a CC BY license

(Creative Commons Attribution 4.0 International License)

<https://creativecommons.org/licenses/by/4.0/>

along with ionization generated by MNBs upon rupture, can break down ozone to produce reactive oxygen species (ROS), thereby accelerating pollutant degradation. Additionally, the active sites on the catalyst surface can adsorb ozone and catalyze the generation of ROS. Coupling these two technologies significantly enhances the rate of pollutant degradation.

**Abstract:** Micro-nano bubbles (MNBs) technology significantly enhances ozone dissolution, prolongs its residence time in aqueous solutions, and expands the contact area between ozone and organic pollutants, thereby improving ozone utilization efficiency. The collapse of MNBs generates hydroxyl radicals ( $\cdot\text{OH}$ ), which synergistically enhance the degradation of organic contaminants via catalytic ozonation. When combined with catalysts, ozone MNBs enable efficient pollutant mineralization across a wide pH range while minimizing ozone and catalyst consumption. This process is effective in a wide pH range, and the catalyst remains active after repeated use. This paper introduces the basic characteristics of micro-nano bubbles and ozone catalytic oxidation technology, focusing on the advantages and disadvantages of ozone micro-nano bubbles and catalytic ozonation in the degradation of organic wastewater, and summarizes the synergistic application of the two technologies in organic wastewater treatment. Meanwhile, the research progress of new catalysts, the energy consumption of micro-nano bubble generation equipment, and the future development of this technology in actual industrial operations are outlined.

**Keywords:** micro-nano bubbles, ozone catalytic oxidation, organic wastewater, hydroxyl radical, catalyst

## 1. Introduction

The rapid advancement of industrialization and urbanization, coupled with population growth, has substantially elevated wastewater discharge standards and global demand for clean water resources. This intensifies the urgency to enhance wastewater treatment efficacy and mitigate water scarcity challenges.<sup>1</sup> Organic wastewater, containing persistent organic compounds, heavy metal ions, and other hazardous contaminants, presents severe environmental risks if improperly discharged. Such effluents contribute to widespread pollution of aquatic systems, soil, and air, thereby disrupting ecological equilibrium and posing critical threats to human health.<sup>2,3</sup> Conventional treatment methods, characterized by inefficiency and high energy consumption, remain inadequate for addressing these challenges. Consequently, the development of efficient, sustainable, and cost-effective organic wastewater treatment technologies has emerged as a global priority in scientific and engineering communities.

Micro-nano bubbles (MNBs) technology is an innovative method for treating organic wastewater that has attracted significant research interest because of its unique properties and potential. MNBs are tiny bubbles with diameters ranging from tens of nanometers to tens of micrometers. Compared to conventional large bubbles, MNBs are smaller, possess a larger specific surface area, exhibit higher mass transfer efficiency, have a longer residence time (slow rate of rise), and display a high interfacial Zeta potential.<sup>4-6</sup> These characteristics make them ideal for oxygen transport. Additionally, during the rupture process, MNBs generate hydroxyl radicals ( $\cdot\text{OH}$ ), superoxide radicals ( $\text{O}_2^{\cdot-}$ ), and other free radicals with strong oxidizing properties, which can rapidly oxidize and degrade pollutants in organic wastewater.<sup>7,8</sup> MNBs effectively break down the chemical bonds of organic molecules, mineralizing them into smaller, simpler compounds, thus facilitating the degradation of organic wastewater.

Ozone catalytic oxidation technology leverages the decomposition of ozone to generate reactive oxygen radicals.<sup>9</sup> This process employs ozone as a strong oxidizing agent, and in the presence of a catalyst, it enhances the efficiency of oxidizing organic matter and other pollutants.<sup>10</sup> Catalysts reduce the decomposition energy of ozone, enhance its oxidizing power, and increase the selectivity of the treatment process, resulting in the effective removal of specific pollutants. Ozone catalytic oxidation technology provides advantages such as high efficiency, rapid action, and absence of secondary pollution, while also demonstrating superior performance compared to traditional oxidation technology for certain specific pollutants.<sup>11</sup>

By separately exploring the advantages and disadvantages of each technology for organic wastewater treatment and combining the characteristics of micro-nano bubbles with ozone catalytic oxidation technology, we can analyze the principles, features, and benefits of these technologies. Furthermore, the effectiveness and feasibility of this

technology in treating organic wastewater can be evaluated through relevant experiments. Simultaneously, we explore the challenges this technology may face in practical applications and its future development. This paper serves as a reference for enhancing the efficiency of organic wastewater treatment, lowering treatment costs, and protecting the environment. Additionally, it promotes the development and application of related technologies.

## 2. Characteristic

### 2.1 Micro-nano bubbles

MNBs are tiny bubbles that exist at the micron and nanometer scales within aqueous solutions, exhibiting unique physical and chemical properties.<sup>12</sup> Compared to traditional large bubbles, MNBs offer several significant advantages due to their small size, including an extended residence time in the liquid because of their slow rise rate,<sup>13</sup> a large specific surface area,<sup>14</sup> a high mass transfer rate,<sup>15</sup> the ability to generate hydroxyl radicals,<sup>16</sup> and a notably high interfacial zeta potential.<sup>17</sup> Figure 1 provides a comparative overview of the size and key properties that distinguish MNBs from conventional bubbles.

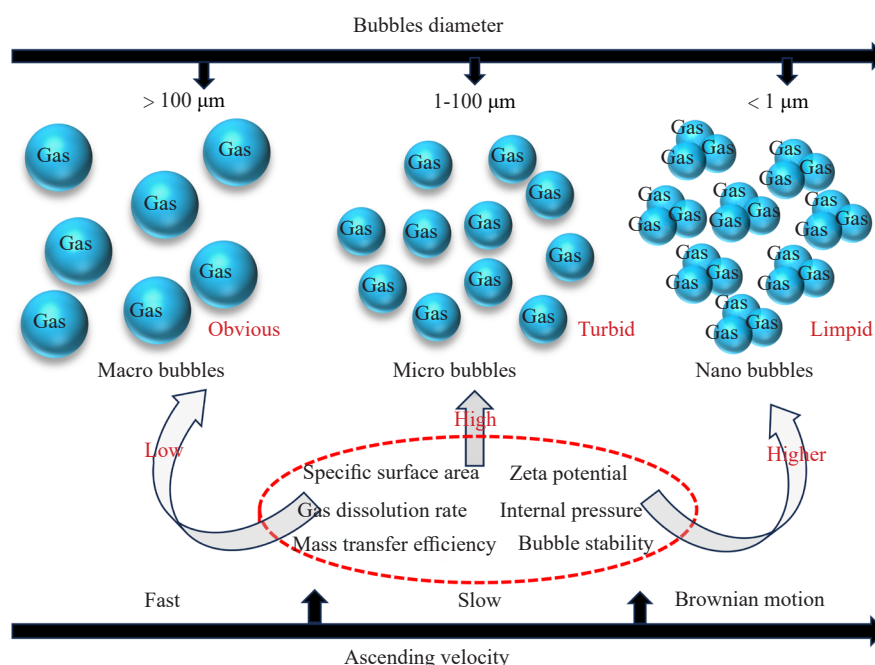


**Figure 1.** Schematic representation of the size range and key properties between conventional bubbles and micro-nano bubbles

#### 2.1.1 Preparation and size distribution

Characterizing the size and size distribution of MNBs is crucial for understanding their performance. Currently, the primary characterization instruments include a nanoparticle tracking analyzer (NTA), focused beam reflectance meter (FBRM), electron microscope (EM), dynamic light scattering (DLS for bubbles ranging from 0.3 nm to 6 μm), particle sizer (for bubbles ranging from 0.5 to 500 μm), and cryo-scanning electron microscope (Cryo-SEM). The principles for preparing MNBs generally include the dispersed air method (mechanical shear method), dissolved air release method, ultrasonic cavitation method, and electrolysis method. Variations in the size distribution of MNBs can arise from different preparation principles and conditions.

The dispersed air method for generating microbubbles (MNBs) utilizes microporous structures and mechanical shear devices to create shear forces that effectively pulverize the air within the water.<sup>18</sup> This process results in the

formation of a substantial number of MNBs. Key factors influencing the properties of MNBs prepared by this method include the volume of aeration, preparation duration, type of bubble generator, inner diameter of the Venturi tube, aperture size of the bubble generator, hydrogen bonding interactions, type of gas used, and gas saturation concentration. These factors significantly affect the concentration, size, surface charge, quantity, and stability of the MNBs. The dissolved gas release method for preparing MNBs relies on the initial step of mixing gas with water under high pressure, resulting in the gas being fully dissolved to create saturated dissolved gas water.<sup>19</sup> Rapidly reducing the pressure to atmospheric levels decreases the solubility of the gas, creating supersaturated conditions. Consequently, the gas precipitates from the solution, forming nanobubbles. The effectiveness of this method depends on variables such as the type of gas, its solubility, the decompression rate, and the aeration apparatus. Ultrasonic cavitation employs high-frequency compression and low-frequency expansion of ultrasound in liquids, causing local pressure to drop below vapor pressure and forming cavities that rapidly collapse and burst, thereby generating MNBs.<sup>20</sup> Electrolysis for MNB production involves placing electrodes within an electrolyte solution. Once energized, these electrodes facilitate redox reactions at their poles, causing the gases at the cathode and anode to become supersaturated and yield H<sub>2</sub> and O<sub>2</sub> MNBs, respectively.<sup>21</sup> The concentration distribution of these bubbles is influenced by the choice of electrolyte, energy consumption of the electrochemical process, and diameter of the electrodes. Table 1 presents the preparation principles, methods, and size distribution of micro-nano bubbles.

### 2.1.2 Long residence time

The rate of rise of MNBs in solution follows Stokes' equation:  $R = \rho g d^2 / 18\mu$  (where  $\rho$  = liquid density,  $g$  = gravitational acceleration,  $d$  = bubble diameter,  $\mu$  = viscosity).<sup>22,23</sup> According to the formula, a smaller bubble diameter results in a slower rate of rise and a longer residence time. The state of MNBs depends on the interaction between the concentration of the bulk dissolved gas and its concentration (denoted as  $f$ ) at the bubble-liquid interface.<sup>24</sup> When  $f > 1$ , the bubble increases in size and eventually bursts. When  $f < 1$ , the gas dissolution rate increases, the bubble volume decreases, and the bubble can remain stable in solution for months.

### 2.1.3 Large specific surface area

MNBs have a larger specific surface area compared to conventional large bubbles, enabling greater contact between gas and solution, thereby accelerating the rate of mass transfer. The specific surface area of a bubble is related to its diameter by the equation  $S = 3V/r$  (where  $V$  is the volume in m<sup>3</sup>,  $S$  is the surface area in m<sup>2</sup>, and  $r$  is the radius in meters). For a given volume, the specific surface area of a bubble is negatively correlated with its diameter: The smaller the bubble diameter, the larger the specific surface area and the faster the mass transfer rate.<sup>25</sup>

### 2.1.4 Hydroxyl radical

MNBs generate substantial amounts of strong oxidizing radicals, such as  $\cdot\text{OH}$ , upon rupture. According to the Young-Laplace relation  $\Delta P = 2\sigma/r$  (where  $\Delta P$  is the pressure variable in  $N$ ,  $\sigma$  is the surface tension in 10<sup>-3</sup> N/m, and  $r$  is the radius in meters), the internal pressure of the bubble is inversely related to its diameter. When the bubble rapidly contracts and ruptures, the pressure and temperature inside increase sharply to a maximum,<sup>26,27</sup> resulting in a thermal decomposition reaction that forms  $\cdot\text{OH}$ .<sup>28</sup> Additionally, when the bubble diameter is less than 10  $\mu\text{m}$ , the concentration of charged ions in the double electric layer rapidly increases and peaks upon rupture. The high concentration of charged ions at the gas-liquid interface releases significant chemical energy, decomposing oxygen molecules to produce reactive oxygen radicals, the most important of which are  $\cdot\text{OH}$ .<sup>29,30</sup> Figure 2 illustrates the process of  $\cdot\text{OH}$  generation from the rupture of MNBs.

### 2.1.5 Zeta potential

Zeta potential is the potential difference arising from the formation of a double electric layer due to the combination of positive and negative ions on the inner and outer surfaces of the bubble, serving as an important indicator of the stability of MNBs.<sup>31</sup> Zeta potential correlates with the adsorption capacity at the bubble interface: The higher the zeta potential, the stronger the adsorption capacity, with the bubble achieving the highest zeta potential at

the moment of rupture. Bubbles with the same charge exhibit mutual repulsion, preventing aggregation and enhancing bubble stability.<sup>32,33</sup> The zeta potential decreases as the electrolyte concentration increases, and its change also depends on the pH and cation valence in the solution.<sup>32</sup> When the solution pH is  $\geq 4$ , the surface of MNBs becomes negatively charged, dominated by OH<sup>-</sup>, which can adsorb low-valent cations. However, when high-valent cations are adsorbed, they can neutralize or reverse the bubble charge, reducing the zeta potential at the bubble interface and destabilizing the bubbles.<sup>34</sup> As the temperature increases, the size of MNBs enlarges, and the zeta potential decreases.<sup>1,35</sup>

**Table 1.** List of micro-nano bubbles preparation and size distribution

Principle	Method	Gas type	Size distribution	Indicator	Conclusion
Distributed Air Method	Venturi Tubular Bubble Generator <sup>20</sup>	Atmosphere	1-100 $\mu\text{m}$ 50-500 nm	FBRM, NTA	By increasing the preparation time and aeration, the concentration of MNBs first increased and then decreased, while the particle size exhibited an opposite trend. Ultimately, the bubble size ranged from 1 to 100 $\mu\text{m}$ and from 50 to 500 nm, while the surface tension also increased.
	Injection Method <sup>36</sup>	Atmosphere	0-10 $\mu\text{m}$	NTA	The particle size of MNBs initially decreases and then increases as the inner diameter of the venturi tube is increased from 2.7 mm to 2.9 mm. Conversely, the particle size increases with the aperture size as the bubble generator's aperture increases from 0.7 mm to 0.9 mm. The micro-nano bubbles produced by this method have a relatively narrow distribution range, with the diameter peak concentrated primarily between 0 and 10 $\mu\text{m}$ , accounting for 97% of the total bubble count.
	Countercurrent Hydrodynamic Cavitation Generator <sup>37</sup>	Atmosphere, O <sub>2</sub>	190-680 nm	DLS	The particle size of NBs was negatively correlated with production time, and bubble size remained constant after saturation. Air nanobubbles averaged 850 nm, while O <sub>2</sub> nanobubbles averaged 650 nm after 10 minutes, exhibiting high O <sub>2</sub> zeta potentials and smaller particle sizes.
Dissolved Gas Release Method	Cycle-Variant Method <sup>38</sup>	N <sub>2</sub> , O <sub>2</sub> , CO <sub>2</sub>	CO <sub>2</sub> : 41-338 nm O <sub>2</sub> : 52-380 nm N <sub>2</sub> : 68-397 nm	DLS EM	Bubble size is positively correlated with both solubility and diffusion capacity. CO <sub>2</sub> is the most soluble, followed by O <sub>2</sub> , while N <sub>2</sub> is the least soluble; all three can remain in solution for up to 48 hours.
	Microbubble Release Heads with Venturi Tube Structure <sup>39</sup>	O <sub>3</sub>	Mainly 5-40 $\mu\text{m}$ , 15-20 $\mu\text{m}$ accounted for 38%, average particle size 20.37 $\mu\text{m}$	EM	Bubble size increases with larger aeration head apertures and higher gas flow rates. The bubble size produced by the microbubble generator was 1/49.09 and 1/245.46 times smaller than that of the bubbles generated by aeration heads with pore sizes of 1 $\mu\text{m}$ and 100 $\mu\text{m}$ , respectively.
Ultrasonic Cavitation	Ultrasonic Treatment of Ultrapure Water <sup>40</sup>	Atmosphere	90-100 nm, bubble concentration of $1.5 \times 10^9 \text{ mL}^{-1}$	DLS, EM	Bubble concentration and generation rate increased with higher ultrasonic power and lower frequency.
	Ultrasonic Treatment of Deionized Water <sup>41</sup>	Atmosphere	0~300 nm	NTA	Bubble size and concentration increase with temperature, ranging from 0 to 300 nm at 25 to 75 °C. Larger bubbles form at lower temperatures due to decreased dissolved gas, which reduces NB concentration through diffusion and aggregation.
Electrolysis	Platinum electrode, NaCl solution <sup>42</sup>	O <sub>2</sub> , H <sub>2</sub>	Less than 100 nm, bubble concentration $5 \times 10^8 \text{ mL}^{-1}$	NTA, DLS	Bubbles were generated by the electrolysis of a NaCl solution with a platinum electrode spacing of 2.79 mm, a voltage of 24 V, and a flow rate of 7.5 mL/s. The solution was then filtered through 20 nm and 450 nm filters, promoting the supersaturation of H <sub>2</sub> and O <sub>2</sub> , leading to bubble formation.



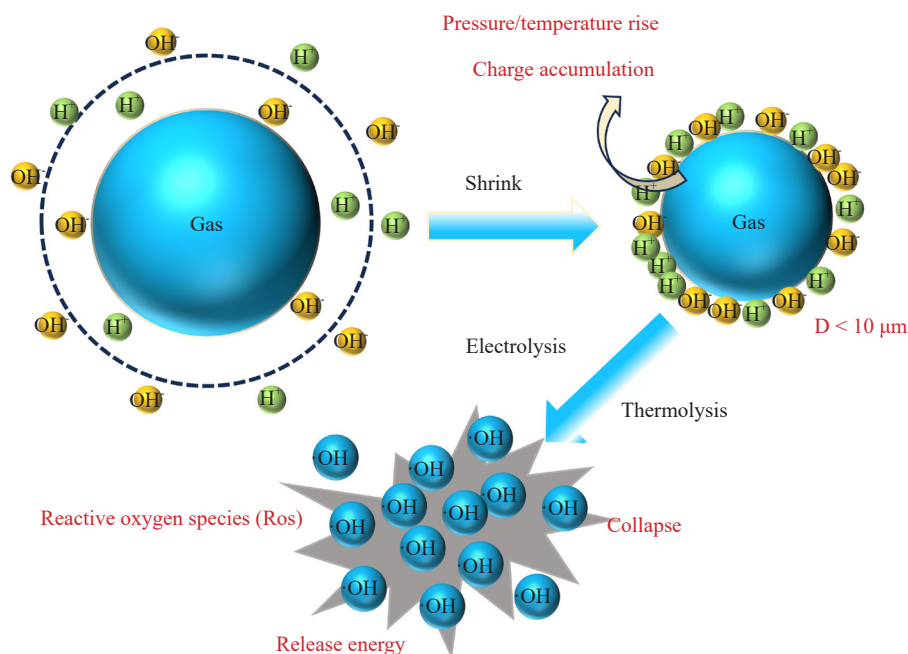


**Figure 2.** Schematic diagram of hydroxyl radical generation by rupture of micro-nano bubbles

## 2.2 Ozone catalytic oxidation

Ozone is a strong green oxidant with few by-products and minimal secondary pollution. In the treatment of organic wastewater, ozone can be divided into direct and indirect reactions. Direct reactions involve the oxidative decomposition of organic matter due to the strong oxidizing properties of ozone, typically characterized by redox and addition-substitution reactions,<sup>43,44</sup> as expressed in reaction equations (1)-(2).<sup>45</sup> Indirect reactions involve the production of singlet oxygen,  $\cdot\text{OH}$  radicals, and other strong oxidizing radicals when ozone is dissolved in an aqueous solution. These radicals can accelerate the oxidative decomposition of organic matter in water, and the by-products of these reactions are less harmful to the environment, as shown in reaction equations (3)-(8). However, ozone has disadvantages, including low reaction efficiency, poor retention capacity, and low production of  $\cdot\text{OH}$  radicals when directly treating organic wastewater.<sup>46</sup> Additionally, unreacted ozone can be harmful to the environment and human health. The reaction processes are illustrated in Figure 3.

Direct reaction:

Under alkaline conditions, pollutants become ionized and acquire a negative charge. Ozone acts as an electrophilic reagent, degrading pollutants by attracting these negatively charged species and targeting areas of high electron cloud density in the pollutants (e.g., double bonds or aromatic rings) through electrophilic addition and substitution reactions.<sup>47</sup>



Equation:

$H-X$ : Organic pollutants (e.g., phenols).

$X^-$ : The negative ion form of a pollutant after ionisation under alkaline conditions.

*Products*: Production of pollutants oxidised by ozone.

Indirect reaction (Take metal oxides as an example):

Ozone introduces oxygen groups to the surface of metal oxides by reacting with  $\cdot\text{OH}$  radicals present on the oxide

surfaces. Metal ions in varying valence states transfer electrons from the catalyst surface to ozone molecules via valence cycling. These processes decompose ozone to generate reactive oxygen species as intermediates.<sup>48</sup> The reactive oxygen species intermediate eventually reacts with water and ozone to ultimately yield reactive oxygen species.



Equation:

*M*: Metal oxides.

*M-OH*: Hydroxyl groups on the surface of metal oxides.

*M-O*: Oxygen groups on the surface of metal oxides (Intermediate states on the surface of the reacted metal oxide).

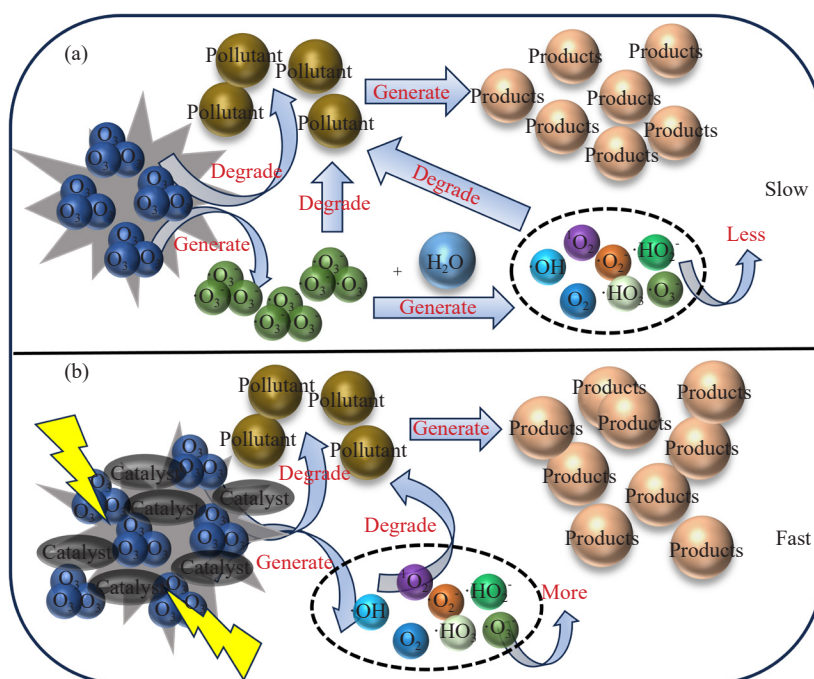


**Figure 3.** Schematic diagram of the mechanism of ozone treatment of organic pollutants. (a) single ozonation (b) catalytic ozonation

Ozone catalytic oxidation is an advanced oxidation technology that relies on the decomposition of ozone in water to generate reactive oxygen radicals and facilitate the oxidative degradation of organic matter using various types of

catalysts.<sup>49</sup> Catalysts provide active sites that lower the energy threshold for ozone decomposition and enhance the production of  $\cdot\text{OH}$  radicals, resulting in a significantly higher reaction rate for the oxidative decomposition of organic matter compared to ozone oxidation alone. Additionally, organic matter can be adsorbed onto the catalyst, enhancing contact between the organic matter and ozone, thereby accelerating mineralization and decomposition. This technology improves selectivity for specific organic compounds, increases mineralization capacity and ozone utilization for targeted organics, and reduces overall process costs.

Ozone catalytic oxidation technology is categorized into homogeneous and heterogeneous processes. Homogeneous ozone catalytic oxidation primarily uses catalysts in the form of metal ions, enhancing the decomposition efficiency of organic matter and improving overall mineralization capacity. However, these catalysts are dissolved in solution, making their recycling and reuse challenging and posing potential environmental pollution risks. Heterogeneous ozone catalytic oxidation technologies primarily utilize solid catalysts, including those with transition metal elements like Fe, Cu, Al, and Mn, as well as rare earth elements such as Ce, metal oxide catalysts, and composite metal catalysts. These catalysts facilitate the catalytic oxidation of organic matter in water. These metals possess empty electron orbitals that can easily form electron pairs, making them ideal catalysts for ozone catalytic oxidation.<sup>50</sup> Such catalysts address the issue of the former's inability to be recycled and reused while maintaining good efficiency in the ozone decomposition of organic matter even after repeated use.<sup>51</sup>

### 3. Ozone micro-nano bubbles for organic wastewater treatment

In industrial applications, conventional ozone treatment of organic wastewater involves using an ozone generator to introduce ozone into the solution in the form of macro bubbles ( $\text{O}_3/\text{MaBs}$ ). However, this method has drawbacks, including low ozone mass transfer efficiency and short residence time, leading to reduced ozone utilization. Ozone micro-nano bubbles ( $\text{O}_3/\text{MNBs}$ ) significantly enhance the solubility of ozone in water and improve its mass transfer efficiency by a factor of 1.3 to 19.<sup>52,53</sup> Compared to conventional ozone oxidation for pollutant degradation,  $\text{O}_3/\text{MNBs}$  can reduce ozone dosage, enhance ozone utilization, and lower costs. The high specific surface area of micro-nano bubbles increases the contact area between ozone and pollutants, thereby enhancing the oxidative degradation of pollutants. Furthermore, enhanced reactive oxygen species (ROS) signals have been observed for  $\text{O}_3/\text{MNBs}$  compared to  $\text{O}_3/\text{MaBs}$  when using dimethyl pyridine N-oxide (DMPO) and 2,2,6,6-tetramethyl-4-piperidine (TEMP) as trapping agents, demonstrating that ROS can be generated by this system. It has also been shown that predominantly  $\cdot\text{OH}$  radicals are involved, as determined by electron paramagnetic resonance (EPR) mapping assays.<sup>54,55</sup> The mechanism of  $\cdot\text{OH}$  generation from  $\text{O}_3/\text{MNBs}$  involves a high concentration of  $\text{OH}^-$  on the surface of negatively charged MNBs, which accelerates the decomposition of ozone to produce  $\cdot\text{OH}$ . Additionally, the collapse and rupture of  $\text{O}_3/\text{MNBs}$  generate high temperature, high pressure, and instantaneous ionization, further decomposing ozone to produce  $\cdot\text{OH}$ .<sup>56</sup>  $\cdot\text{OH}$  possesses stronger oxidizing properties than  $\text{O}_3$  and can non-selectively degrade pollutants, while  $\text{O}_3$  is more selective. Therefore,  $\text{O}_3/\text{MNBs}$  have a distinct advantage in treating pollutants that are difficult to degrade.<sup>57</sup>  $\text{O}_3/\text{MNBs}$  do not require the addition of other agents, thereby avoiding secondary pollution to the environment.<sup>58</sup> The contribution of each reactive oxygen radical in the ROS to pollutant removal, as well as the  $\text{O}_3$  utilization rate, can be calculated using equations (9)-(11).<sup>55,59</sup> The differences between  $\text{O}_3/\text{MNBs}$  aeration and conventional bubble aeration are illustrated in Figure 4.



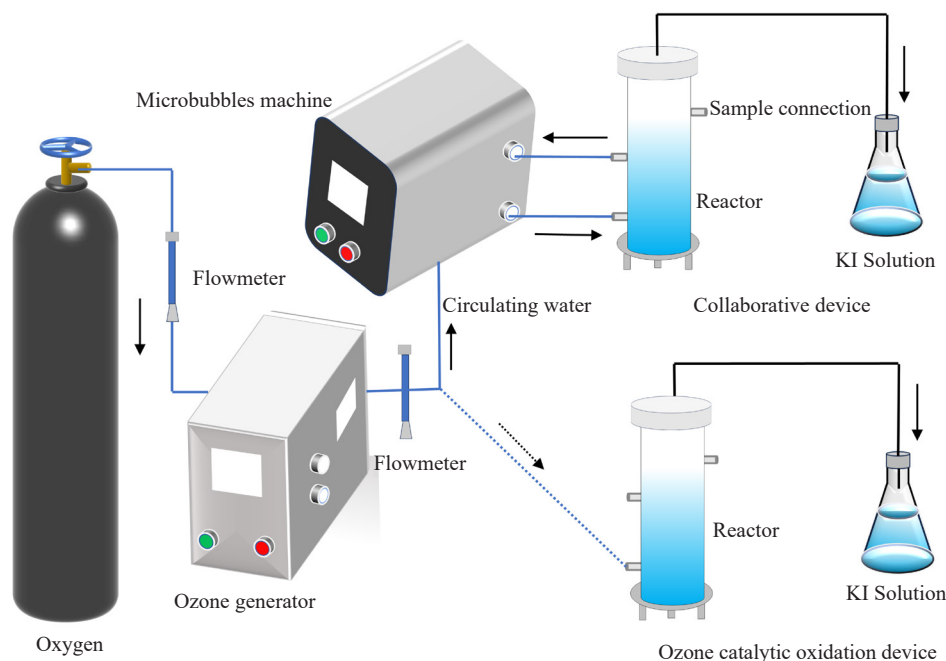


**Figure 4.** Schematic diagram of ozone microbubble (upper part) and conventional bubble (bottom part) aeration systems

ROS pollutant removal contribution rate formula:

The selection of the corresponding quencher is contingent upon the specific ROS targeted for detection. The contributions of different ROS to pollutant degradation are calculated as percentages.

$$\lambda_{\cdot OH} = \frac{k_M - k_{TBA}}{k_M} \times 100\% \quad (9)$$

$$\lambda_{^1O_2} = \frac{k_{TBA} - k_{L-Histidine}}{k_M} \times 100\% \quad (10)$$

$$\lambda_{O_2^{\cdot -}} = \frac{k_{L-Histidine} - k_{PBQ}}{k_M} \times 100\% \quad (11)$$

Formula:

$M$ : Organic pollutant.

$\lambda$ : The contribution of different ROS to the removal of  $M$  (%).

$k$ : The first-order reaction kinetic constant for  $M$  removal in the presence of each reactive oxygen radical in ROS ( $\text{min}^{-1}$ )

TBA: Quenchers of  $\cdot OH$

L-Histidine: Quenchers of  $\cdot OH$  and  $^1O_2$

PBQ: Quenchers of  $\cdot OH$ ,  $^1O_2$  and  $O_2^{\cdot -}$

$O_3$  utilization formula:

Based on the known total ozone dosage, the liquid-phase ozone concentration and the escaped ozone concentration during the experiment are calculated to determine the actual ozone concentration involved in the degradation of pollutants, thereby enabling the calculation of ozone utilization efficiency.

$$\eta = \left( 1 - \frac{A_1 + A_2}{A_0} \right) \times 100\%$$

Formula:

$\eta$ : O<sub>3</sub> utilization rate (%).

$A_0$ : The total amount of O<sub>3</sub> passed through at moment  $t$  (mg).

$A_1$ : The amount of liquid phase O<sub>3</sub> at moment  $t$  (mg).

$A_2$ : The cumulative gas-phase O<sub>3</sub> fugitive volume at moment  $t$  (mg).

Using O<sub>3</sub> combined with micro-nano bubbles (MNBs) to treat real wastewater results in changes in pH having a minimal effect on pollutant degradation efficiency. The production of  $\cdot\text{OH}$  by O<sub>3</sub>/MNBs primarily relies on the high temperature and pressure generated during bubble rupture and ionization, with this effect being more pronounced under acidic conditions.<sup>58,59</sup> While  $\cdot\text{OH}$  reacts with excess OH<sup>-</sup> under alkaline conditions, it also generates other reactive oxygen species (ROS) that degrade pollutants, such as O<sub>2</sub><sup>-</sup> and HO<sub>2</sub><sup>-</sup>.<sup>60,61</sup> In industrial applications, the nature of the contaminant can have a greater influence on degradation efficiency than pH conditions. Aromatic compounds are more susceptible to attack by O<sub>3</sub> and  $\cdot\text{OH}$  in acidic conditions, particularly in electron-rich regions such as double bonds or substituents.<sup>62</sup> Aliphatic compounds are inefficiently oxidized directly by O<sub>3</sub> and react with  $\cdot\text{OH}$  under alkaline conditions.  $\cdot\text{OH}$  efficiently oxidizes aliphatic compounds through hydrogen extraction or addition reactions.<sup>63</sup>

O<sub>3</sub>/MNBs and O<sub>3</sub>/MaBs have been employed to degrade phenol and nitrobenzene in wastewater. It was concluded that phenol was degraded by reaction with O<sub>3</sub>, while nitrobenzene was degraded by reacting with ROS generated from the decomposition of O<sub>3</sub>. Moreover, the degradation rate of organic matter by O<sub>3</sub>/MNBs was 2.00 to 3.37 times higher than that of the O<sub>3</sub>/MaBs system across pH levels of 3 to 11. A high concentration of O<sub>3</sub> harnesses the energy released by the collapse of MNBs to rapidly activate in the presence of a large number of OH<sup>-</sup> ions, generating  $\cdot\text{OOH}$  and consequently  $\cdot\text{OH}$ . The degradation rate of nitrobenzene dropped from 87.8% to 57.2% and 33.3% with the addition of TBA and ascorbic acid, respectively, demonstrating that ROS were generated in the O<sub>3</sub>/MNBs system. O<sub>2</sub><sup>-</sup> degraded nitrobenzene at a higher rate than  $\cdot\text{OH}$ , with <sup>1</sup>O<sub>2</sub> contributing 14.6% to the degradation of nitrobenzene. The O<sub>3</sub> utilization rate exceeded 90%.<sup>59</sup>

The efficiencies of O<sub>3</sub>/MNBs and O<sub>2</sub>/MNBs for PVA degradation were compared, revealing that O<sub>3</sub>/MNBs removed 98.58% of PVA, while O<sub>2</sub>/MNBs removed only 48.68%. O<sub>2</sub>/MNBs primarily relied on air flotation to degrade PVA, whereas O<sub>3</sub>/MNBs generated more ROS in solution and combined it with air flotation for PVA treatment. The COD removal rate of O<sub>3</sub>/MNBs reached 75.6% at pH 8.69, which was 33.2% higher than the rate at pH 3.30.<sup>64</sup>

O<sub>3</sub>/MNBs were employed to degrade sulfamethoxazole (SMX). SMX was nearly fully degraded by O<sub>3</sub>/MNBs within 30 minutes, while the removal rate of SMX by O<sub>3</sub>/MaBs was only 56.83%. Additionally, the removal rate of TOC by O<sub>3</sub>/MNBs after 90 minutes was 32.42%, compared to only 9.80% for the O<sub>3</sub>/MaBs system. The degradation and mineralization rates of SMX in the O<sub>3</sub>/MNBs system were 3.26 and 4.10 times higher, respectively, than those in the O<sub>3</sub>/MaBs system. The burst reactions with TBA and L-Histidine resulted in 84.82% and 67.74% removal of SMX by  $\cdot\text{OH}$  and <sup>1</sup>O<sub>2</sub>, respectively. The concentration of dissolved O<sub>3</sub> in the O<sub>3</sub>/MNBs system and the amount of accumulated exhaust O<sub>3</sub> were measured, yielding a final O<sub>3</sub> utilization rate of 83.30%.<sup>55</sup>

The coupled electrolysis of O<sub>3</sub>/MNBs to generate H<sub>2</sub>O<sub>2</sub> was employed to degrade CIP, which could be completely degraded within 60 minutes under the conditions of an O<sub>3</sub> dosage of 12.5 mg/min, an applied current of 50 mA, and pH 7.0. In contrast, the degradation rates of CIP after 90 minutes were only 9.91% for electrolysis alone and 73.47% for O<sub>3</sub>/MNBs. The coupled system generates H<sub>2</sub>O<sub>2</sub> at the cathode, promoting the decomposition of O<sub>3</sub> to produce  $\cdot\text{OH}$ , with the corresponding ozone utilization rate approaching 100%. The reactive oxygen radical burst using PBQ, L-Histidine, and TBA indicated that  $\cdot\text{OH}$ , <sup>1</sup>O<sub>2</sub>, O<sub>3</sub>, and O<sub>2</sub><sup>-</sup> contributed 66.79%, 23.57%, 6.67%, and 2.98%, respectively, to CIP removal.<sup>65</sup>

O<sub>3</sub>/MNBs were used to oxidatively degrade a typical UV filter, Diethylamino Hydroxybenzoyl Hexyl Benzoate (DHBB), achieving a removal rate of 87.3% within 60 minutes at 25 °C, an ozone concentration of 10.22 mg/L, and a pH of 11. This removal effect was 2.02 times greater than that of conventional ozone bubbles. Bursting experiments with the addition of TBA and PBQ led to 65.2% degradation of DHBB by  $\cdot\text{OH}$  and 14.9% degradation by O<sub>2</sub><sup>-</sup>. The  $\cdot\text{OH}$  exposure in the O<sub>3</sub>/MNBs system was 70.8% higher than in the O<sub>3</sub>/MaBs system, and the ozone utilization rate was 38% higher, as measured using the p-CBA probe.<sup>66</sup>

Compared to  $O_3$ /MaBs and  $O_3$ /MNBs in treating organic wastewater,  $O_3$ /MNBs offer advantages by increasing the residence time of  $O_3$  in solution and enhancing the contact area with organic matter. Additionally,  $O_3$  combined with MNBs stimulates the generation of a large number of strongly oxidizing ROS, accelerating the oxidative degradation of organic matter. The removal rate of each reactive oxygen radical in pollutant degradation can be calculated through bursting experiments, with the  $\cdot OH$  radical playing a primary role.  $O_3$ /MNBs demonstrate effective performance in the oxidative degradation of organic matter across a wide pH range. This indicates that  $O_3$ /MNBs technology is more cost-effective and holds greater value for applied research.

## 4. Ozone catalytic oxidation technology for organic wastewater treatment

Non-homogeneous ozone catalytic oxidation technology utilizing solid catalysts can accelerate the mass transfer rate of ozone, enhance ozone utilization, and promote the degradation and treatment of organic wastewater, which can be recycled and reused for secondary purposes, thereby avoiding environmental pollution caused by metal ions. Commonly used solid-state catalysts include monometallic catalysts, supported metal catalysts, composite metal catalysts, and non-metallic catalysts. The mechanism of organic matter degradation through catalytic ozonation is illustrated in Figure 5.

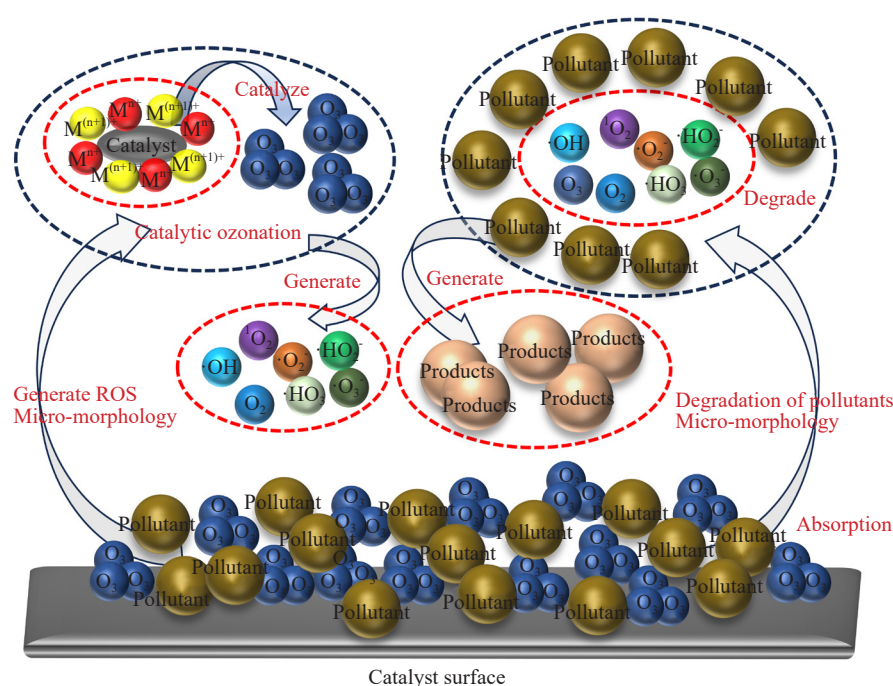


**Figure 5.** Schematic diagram of the mechanism of degradation of organic matter by catalytic ozonation

### 4.1 Monometallic catalysts

Monometallic catalysts are created by loading or modifying a single metal or its compound onto a carrier. Compared to ozone oxidation alone, these catalysts can adsorb ozone and promote its decomposition to generate  $\cdot OH$  radicals, reducing the activation energy of the reaction and increasing the reaction rate by utilizing oxygen vacancies on the surface of metal oxides, as well as the electrons and empty orbitals provided by the metal ions and the hydroxyl groups on the catalyst surface as active sites.<sup>67,68</sup> Oxygen vacancies can alter the electron distribution and the characteristics of active sites on the catalyst surface, thereby regulating oxidant activation and pollutant degradation selectivity. Notably, the concentration of oxygen vacancies is directly proportional to the generation of  $\cdot OH$  radicals.<sup>69,70</sup> Lewis acid sites on the catalyst surface act as active sites that accept electron pairs from empty orbitals (e.g., d and p

orbitals). During ozone catalysis, the d orbitals of metal ions interact with the antibonding orbitals of ozone, facilitating the transfer of electrons to these orbitals, which attacks the O = O bond of ozone and promotes its decomposition.<sup>71,72</sup> The efficacy of monometallic catalysts in ozone oxidation for the degradation of organic matter was compared with other reaction systems, as shown in Table 2.

**Table 2.** List of comparative experiments on ozone oxidation catalyzed by monometallic catalysts

Catalytic system	Comparison test	Condition	Conclusions
CeO <sub>2</sub> nanorods/O <sub>3</sub> <sup>73</sup>	Comparison of phenol removal rate with O <sub>3</sub>	Reaction under alkaline condition for 30 min	CeO <sub>2</sub> nanorods catalyze the generation of ·OH from ozone due to the abundance of oxygen vacancies on their surface and the synergistic effect of the Ce <sup>3+</sup> /Ce <sup>4+</sup> redox cycle. The phenol removal efficiency was 100% for CeO <sub>2</sub> nanorods/O <sub>3</sub> and only 83.32% for O <sub>3</sub> .
O <sub>3</sub> /Al <sub>2</sub> O <sub>3</sub> /ZnO <sup>74</sup>	Comparison of phenol removal with O <sub>3</sub> , O <sub>3</sub> /Al <sub>2</sub> O <sub>3</sub> , O <sub>3</sub> /ZnO	The same reaction system for 60 min	The presence of abundant oxygen vacancies and hydroxyl groups on the surface of ZnO nano catalysts with a large specific surface area can adsorb ozone and pollutants, and catalyze the formation of ·OH from ozone. The efficiency of O <sub>3</sub> /Al <sub>2</sub> O <sub>3</sub> /ZnO for phenol removal was 86.8%, while O <sub>3</sub> was only 66.2%.
UV/O <sub>3</sub> /BiPO <sub>4</sub> <sup>75</sup>	Comparison with UV/BiPO <sub>4</sub> and O <sub>3</sub> on the efficiency of treating SDBS	The same reaction system for 75 min	BiPO <sub>4</sub> nanorods produce photogenerated electrons (e <sup>-</sup> ) and holes (h <sup>+</sup> ) upon irradiation with UV or visible light. e <sup>-</sup> reacts with ozone molecules to form ·O <sub>2</sub> <sup>-</sup> and ·OH, h <sup>+</sup> oxidizes surfactant molecules or water molecules to form ·OH. UV/O <sub>3</sub> /BiPO <sub>4</sub> was 4.9 and 3.8 times more efficient than UV/BiPO <sub>4</sub> and O <sub>3</sub> for treating SDBS.
Fe <sub>0.08</sub> /CFA/O <sub>3</sub> <sup>76</sup>	Comparison of CH <sub>3</sub> COONa removal with O <sub>3</sub>	The reaction was carried out for 60 min at a concentration of O <sub>3</sub> of 50 mg·L <sup>-1</sup> under neutral conditions with a catalyst of 3.0 g·L <sup>-1</sup>	The oxygen vacancies on the surface of Fe <sub>0.08</sub> /CFA and the high specific surface area of CFA provide abundant active sites, and the redox cycle of Fe <sup>2+</sup> /Fe <sup>3+</sup> further enhances ozonolysis and ·OH generation. The removal of CH <sub>3</sub> COONa by O <sub>3</sub> was low, while the efficiency of Fe <sub>0.08</sub> /CFA/O <sub>3</sub> in removing CH <sub>3</sub> COONa could reach 53.3%.
Mn-CSM/O <sub>3</sub> <sup>77</sup>		Reaction for 60 min at 2.0 g·L <sup>-1</sup> catalyst	Mn-CSM enhances the catalytic ozone generation of ·OH due to its high specific surface area, abundant active sites, and the redox cycling ability of Mn <sup>2+</sup> /Mn <sup>3+</sup> . The mass transfer efficiency of the reactor is also optimized, allowing ozone to come into full contact with the pollutants. The degradation of oxalic acid by Mn-CSM/O <sub>3</sub> reached 93%, and the COD in the coal wastewater was reduced from 105 mg·L <sup>-1</sup> to 42 mg·L <sup>-1</sup> with a total O <sub>3</sub> migration of 155 mg.

## 4.2 Composite metal catalysts

Composite metal catalysts enhance ozone decomposition and pollutant degradation efficiency through the synergistic effects of multiple metal components. Different metals can facilitate ozonolysis to produce ROS and adsorb pollutants, respectively. The valence change cycle of metal ions promotes the formation of oxygen vacancies and electron transfer, resulting in the generation of more ROS for the efficient degradation of organic pollutants.<sup>78,79</sup> Compared to monometallic catalysts, alloying and interfacial bonding between composite metals reduce metal ion leaching, allowing the catalysts to catalyze ozone across a wide pH range and prolonging catalyst lifetime.<sup>80</sup> Lewis acidity depends on the metal coordination number; the lower the coordination number, the higher the acidity and the greater the number of available empty orbitals.<sup>81</sup> Coordinated use of composite metals reduces the number of metal coordination sites, increases Lewis acid sites, and enhances catalytic ozone performance.<sup>82</sup>

Cu-Ce@ $\gamma$ -Al<sub>2</sub>O<sub>3</sub> was employed as a catalyst for the ozone-catalyzed oxidative degradation of RO concentrate water, utilizing CuO as the active component and CeO<sub>2</sub> to enhance the bond strength between the active component and the  $\gamma$ -Al<sub>2</sub>O<sub>3</sub> carrier. The optimal ozone-catalyzed oxidation process conditions were achieved with an active metal loading ratio of Cu : Ce = 2 : 1, an ozone flow rate of 0.2 L/min, a catalyst filling ratio of 12%, a pH of 9, and a reaction

time of 60 minutes. Under optimal operating conditions, COD removal in RO concentrate water can reach as high as 85.1%, compared to only 18% for ozone oxidation alone.<sup>83</sup>

MgAl<sub>2</sub>O<sub>4</sub> was utilized as a catalyst for the degradation of ibuprofen through ozone-catalyzed oxidation. The removal of ibuprofen at a concentration of 5 mg·L<sup>-1</sup> by MgAl<sub>2</sub>O<sub>4</sub>/O<sub>3</sub> was 74.0%, while total organic carbon (TOC) removal was 68.8%. The pollutant removal rate was maintained at over 67% for 25 hours, significantly outperforming ozone oxidation alone (42.7%) and the Al<sub>2</sub>O<sub>3</sub> membrane (52.1%) for ibuprofen removal.<sup>84</sup>

Cu-Mn/ $\gamma$ -Al<sub>2</sub>O<sub>3</sub> catalysts were employed for the ozone-catalyzed oxidative degradation of poly (vinyl alcohol) in water. A Cu-Mn/ $\gamma$ -Al<sub>2</sub>O<sub>3</sub> (CMA) composite catalyst was prepared using  $\gamma$ -Al<sub>2</sub>O<sub>3</sub> as the carrier and Cu and Mn as the active components. The kinetic rate constants for PVA degradation through ozone-catalyzed oxidation significantly increased compared to ozone oxidation alone. The optimal catalyst dosage was 100 mg·L<sup>-1</sup> at an initial PVA concentration of 20 mg·L<sup>-1</sup>. The removal rates of PVA were 97.8% and 99.3% under neutral conditions and at pH 10, respectively, with the catalysts remaining effective after five repeated uses.<sup>85</sup>

FeCu-C@MS/O<sub>3</sub> was employed as a molecular sieve-type catalyst for the ozone-catalyzed oxidative degradation of Cumyl hydroperoxide (CHP). The FeCu-C@MS/O<sub>3</sub> system operated at an ozone concentration of 20 mg·L<sup>-1</sup>, a catalyst injection of 50 g·L<sup>-1</sup>, at pH 7, and an initial CHP concentration of 12 mg·L<sup>-1</sup>. After a 120-minute reaction, the CHP removal rate can reach 65.47%, which is 35.80% higher than that of the O<sub>3</sub> system alone. After five cycles of use, the CHP removal rate can still reach 55.19%. The highest CHP removal was observed at pH 11, reaching 80.19%.<sup>86</sup>

### 4.3 Non-metallic catalysts

Heat-oxidation-heat modification of activated carbon (AC) was utilized as a catalyst for the ozonation of humic acid (HA) pollutants in water. The ozonation activity of modified AC was superior to that of unmodified AC, with COD removal increasing from 71% to 96% after 10 minutes of reaction, while the removal of COD by ozonation alone was only 56%. This enhancement is primarily attributed to the increased content of ·OH radicals on the surface following AC modification. The modification also restored the catalytic activity of the used AC, increasing COD removal from 74% to 97%.<sup>87</sup>

Ammonia-heated activated carbon fibers at 120 °C for 12 hours were employed as catalysts for the degradation of oxalic acid through ozone-catalyzed oxidation. O<sub>3</sub> oxidative degradation of oxalic acid alone for 60 minutes resulted in only 7% removal, while the addition of unmodified activated carbon fibers resulted in only 50% removal, whereas modified activated carbon fibers achieved a removal rate of 97%.<sup>88</sup>

Compared to the degradation of organic wastewater by ozone oxidation alone, the addition of catalysts in non-homogeneous ozone catalytic oxidation technology can accelerate the catalytic decomposition of O<sub>3</sub>, enhance its oxidative performance, and promote the degradation and mineralization of organic wastewater. Furthermore, the solid non-homogeneous catalyst can be reused multiple times without any significant change in efficiency, thereby avoiding secondary pollution to the environment during the treatment process. However, the limited solubility of O<sub>3</sub> in solution leads to disadvantages such as low O<sub>3</sub> utilization, low mass transfer efficiency, and high costs. Therefore, enhancing O<sub>3</sub> solubility in solution has become a key technological focus.

## 5. Coupled systems for the treatment of organic wastewater

Ozone catalytic oxidation technology can reduce the treatment time of organic wastewater and is environmentally friendly. However, in practice, ozone is typically transferred into the solution in the form of large bubbles, resulting in a short residence time and wastage of ozone. MNBs technology is integrated with ozone catalytic oxidation technology to enhance the residence time of ozone in solution. Additionally, the inclusion of catalysts can promote further generation of hydroxyl (·OH) radicals during the ozone oxidation process, as illustrated in Figure 6, thereby increasing ozone utilization and the degradation of organic matter in the system.



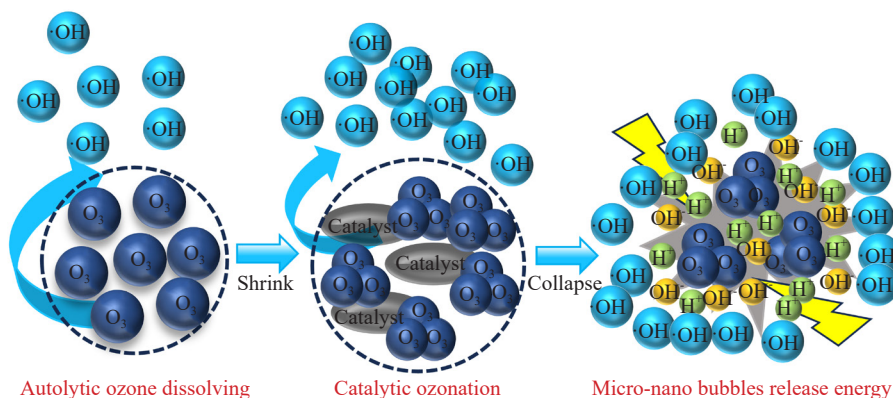


**Figure 6.** Schematic diagram of a catalyst promoting the generation of  $\cdot\text{OH}$  radicals by ozone oxidation of micro-nano bubbles

In this system, composite metal catalysts and loaded metal oxides are commonly employed to enhance ozone decomposition for the production of  $\cdot\text{OH}$ . Commonly used loading materials include carbon-based materials and  $\text{Al}_2\text{O}_3$ , etc.

The advantages of composite metal catalysts are discussed in Section 4.2. However, in actual wastewater treatment processes, the metal active components tend to aggregate, resulting in decreased active site density. Additionally, variations in wastewater characteristics increase the leaching of metal elements, inhibiting catalyst activity.<sup>89</sup> Composite metals loaded with materials disperse the metal active components, improve adsorption capacity, and enhance catalytic performance and stability due to their high specific surface area and porous structure.<sup>90</sup>

Carbon-based carrier catalysts offer numerous active adsorption sites that enhance the adsorption of pollutants and ozone due to their large specific surface area and rich pore structure. They also disperse metal oxides to prevent excessive active site density, thereby maintaining efficient catalytic performance.<sup>91</sup> Its surface oxygen-containing functional groups, free delocalized  $\pi$ -electrons, and carbon defect sites can react with ozone to alter the carbon electronic structure, increase the rate of electron transfer, and promote ozone decomposition.<sup>92,93</sup> Additionally, strong metal-support interaction (SMSI) can occur when metal oxides are loaded, modulating and rearranging the electronic structure through charge transfer between the metal active component and the carrier. This enhances metal-carrier bonding, reduces metal leaching, and prolongs catalyst lifetime.<sup>94,95</sup> Carbon-based carriers exhibit excellent chemical inertness, mechanical stability, and high thermal stability. They maintain good activity under varying pH conditions and can be reused by removing carbon deposits through calcination and acid washing, restoring pore density and surface functional groups.<sup>96,97</sup> Utilizing waste biomass pyrolysis to prepare biocarbon as a carrier aligns with sustainable development goals and reduces costs.<sup>98</sup>

$\text{Al}_2\text{O}_3$  carrier-type catalysts are cost-effective, with  $\gamma\text{-Al}_2\text{O}_3$  or ceramic membranes commonly selected as carriers.  $\gamma\text{-Al}_2\text{O}_3$  possesses a high specific surface area and microporous structure, enhancing ozone and pollutant adsorption, uniformly dispersing metal oxides, preventing active site aggregation, and providing high mechanical strength.<sup>99,100</sup> The surface is rich in  $-\text{OH}$  and Lewis acid sites. These sites can hydrolyze water molecules to generate  $-\text{OH}$  through the coordination effect of unsaturated sites, react with ozone to produce  $\cdot\text{OH}$ , and anchor metal ions to form a stable active center.<sup>101,102</sup> The strong interaction between metal oxides and  $\gamma\text{-Al}_2\text{O}_3$  through metal-oxygen bonding prevents metal particle aggregation and enhances catalytic activity and thermal stability. However,  $\gamma\text{-Al}_2\text{O}_3$  is prone to deactivation in acidic and alkaline environments.<sup>101,103</sup>  $\text{Al}_2\text{O}_3$  ceramic membranes possess a dense crystal structure, superior mechanical strength, thermal stability, and chemical inertness compared to  $\gamma\text{-Al}_2\text{O}_3$ , along with strong corrosion resistance and an extended service life. However, their specific surface area and porosity are relatively low, resulting in slightly weaker adsorption and catalytic properties, which can be optimized by adding pore-forming materials.<sup>104</sup> In practice, suitable  $\text{Al}_2\text{O}_3$  carriers should be selected based on the nature of the wastewater and the treatment method.  $\text{Al}_2\text{O}_3$  carrier catalysts are highly chemically inert and thermally stable, and can be recycled after use by removing carbon deposits through acid washing and calcination, thereby reducing active material clogging.<sup>105</sup>

The micro-nano bubbles coupled with the ozone-catalyzed oxidation system are compared with other reaction systems for the degradation of organic matter, as shown in Table 3.

**Table 3.** List of comparative experiments of ozone-catalyzed oxidation systems with micro-nano bubbles

Catalytic system	Comparison experiment	Experimental condition	Conclusions
LOZO Series Catalyst/ O <sub>3</sub> /MNBS <sup>106</sup>		Ozone concentration 50%, reaction temperature less than 35 °C, reaction time 120 min.	Redox cycling involving polymetallic elements and hydroxyl groups on the catalyst surface enhances ozone decomposition. This catalytic system achieved a 47.7% removal of COD, with a broad range of pH exerting minimal influence on the removal efficiency.
Mn/GAC/O <sub>3</sub> /MNBS <sup>107</sup>	Comparison of chrominance removal with O <sub>3</sub> /MNBS alone	Mn/GAC of 3.5 g·L <sup>-1</sup> , pH 9.4, temperature 23.6 °C.	Redox cycling of multiple valence states during the MnO <sub>2</sub> reaction accelerates electron transfer and enhances the generation of ·OH radicals from ozone molecules. This catalytic system achieved the highest removal rate of 95.6% for dye wastewater chrominance. The combination of unmodified activated carbon (AC) with O <sub>3</sub> /MNBS increased the removal rate by 29%. After five cycles of catalyst recycling, the leaching rate of Mn was only 1.4%, indicating no significant loss of active sites and demonstrating good stability.
MnO <sub>2</sub> /Al <sub>2</sub> O <sub>3</sub> /O <sub>3</sub> /MNBS <sup>108</sup>	Comparison with O <sub>3</sub> /MNBS for quinoline degradation efficiency	The same reaction system was reacted for 60 min and the ozone concentration was 30 mg·L <sup>-1</sup> for 90 min.	Mn exists in multiple oxidation states and can undergo electron transfer reactions through redox cycling, facilitating ozone decomposition and ·OH production. The catalytic system enhanced quinoline removal by 40% at 60 minutes and over 95% at 90 minutes, with ·OH playing a significant role. The catalyst's specific surface area decreased from 183.22 m <sup>2</sup> /g to 175.07 m <sup>2</sup> /g, the average pore volume from 0.27 cm <sup>3</sup> /g to 0.25 cm <sup>3</sup> /g, and the average pore size increased from 4.87 nm to 5.75 nm, indicating that its structure remained largely intact and stable during the reaction.
OHBC/O <sub>3</sub> /MNBS <sup>109</sup>	Comparison of 2,4-D degradation efficiency with O <sub>3</sub> alone	Same conditions.	Oxygen-containing functional groups on the catalyst surface react with ozone to generate ·OH radicals. This catalytic system achieved an 89% efficiency for the degradation of 2,4-D and a 42% removal rate by O <sub>3</sub> /MNBS. After three cycles of reuse, the -OH content on the surface decreased from 1.25 mmol/g to 1.0 mmol/g, yet the removal efficiency of 2,4-D remained at 75.2%, indicating a potential for reuse.
Mn/AC/O <sub>3</sub> /MNBS <sup>110</sup>	Comparison of degradation efficiency of Basic Yellow 28 dye by Mn/AC, Cu/AC, Fe/AC and ozonation alone	Ozone concentration 10.3 mg/L, reaction time 120 min, catalyst dosage 3.0g/L, pH 9.4, reaction temperature 31.7 °C.	Mn has more valence states compared to Cu and Fe, which better facilitates electron transfer reactions through redox cycling and accelerates the generation of ·OH from ozone. The COD and UV <sub>254</sub> removal rates of the Mn/AC catalytic system reached 73.6% and 79.3%, respectively, which were 3.1 times higher than those of the CB/O <sub>3</sub> system. After five cycles of catalyst recycling, the leaching rate of Mn was only 1.4%, the COD removal rate after the fifth use was only 5% lower than that of the first use, while the color removal rate decreased by 6%, indicating no significant loss of active sites and demonstrating good stability.
SBC-LDH/O <sub>3</sub> /MNBS <sup>111</sup>	Rate of removal of tetracycline TCH from wastewater compared to O <sub>3</sub> alone	SBC-LDH of 0.5 g·L <sup>-1</sup> , pH 4.8, ozone dosage 0.3 L/min, TCH 50 mg/L.	Redox cycling involving polymetallic elements and hydroxyl groups on the catalyst surface facilitates ozone decomposition. All ozone microbubble treatment processes achieved nearly 100% removal of TCH, whereas the CB/O <sub>3</sub> and CB/O <sub>3</sub> /SBC-LDH processes resulted in only 34.02% and 62.51% removal, respectively. The primary mechanism for TCH removal is enhanced oxidation facilitated by O <sub>2</sub> · and <sup>1</sup> O <sub>2</sub> . In the five-cycle experiments, TOC removal efficiency dropped from 59.64% in the first cycle to 49.76% in the fifth, with Mn leaching at 47.7 µg/L, indicating that the catalysts maintained high activity during multiple cycles.
O <sub>3</sub> /MNBS/γ-FeOOH/BAF <sup>112</sup>	Removal of COD <sub>Cr</sub> from paper wastewater in comparison with O <sub>3</sub> /MNBS system	pH 7.0, γ-FeOOH/BAF 300 g·L <sup>-1</sup> , ozone dosage 9.9 mg/min.	The Fe-OH groups on the surface of the γ-FeOOH catalyst participate in ozonolysis and MB/O <sub>3</sub> cleavage, promoting the generation of ·OH and accelerating pollutant degradation. When comparing the removal rate of COD <sub>Cr</sub> using the O <sub>3</sub> /MNBS system, this catalytic approach increased the rate from 38% to approximately 60% to 70%. The catalyst demonstrated a stable effect on COD <sub>Cr</sub> removal during 14 days of continuous operation, experiencing no significant deactivation, and the treated COD <sub>Cr</sub> mass concentration met the emission standards. This indicates the good reusability of the catalyst.

Table 3. (cont.)

Catalytic system	Comparison experiment	Experimental condition	Conclusions
MAL/MB/O <sub>3</sub> <sup>113</sup>	Comparison of MAL/CB/O <sub>3</sub> , MB/O <sub>3</sub> and MAL/MB/O <sub>3</sub> on COD concentration changes in wastewater	Actual pharmaceutical wastewater, reaction time 90 min, ozone flow rate 0.5 L/min, ozone dosage to total COD ratio about 0.6, MAL of 0.5 g·L <sup>-1</sup> .	The bimetallic structure accelerates the electron transfer rate, offers a high specific surface area, and provides abundant pore space, thereby promoting pollutant adsorption and catalytic ozonation. The ratios of COD removal to ozone depletion were 0.60, 0.62, and 0.83, respectively; MAL/MB/O <sub>3</sub> achieved a COD removal of 49.79%.
MnCo <sub>2</sub> O <sub>4</sub> /CM/MB/O <sub>3</sub> <sup>114</sup>	Comparison of the degradation rate of BPA by CM/MB/O <sub>3</sub> , MnCo <sub>2</sub> O <sub>4</sub> /CM/MB/O <sub>3</sub> , titanium alloy/O <sub>3</sub>	Ozone flow rate of 40 ml/min, ozone dosing of 2 g/h, reaction time 60 min, pH 7.0.	MnCo <sub>2</sub> O <sub>4</sub> /CM exhibits a high specific surface area, facilitates electron transfer through the redox cycling of Co <sup>2+</sup> /Co <sup>3+</sup> , and serves as a Lewis acid site for the generation of ·OH and O <sub>2</sub> <sup>·-</sup> . MnCo <sub>2</sub> O <sub>4</sub> /CM/O <sub>3</sub> achieved a BPA degradation efficiency of 90% within 60 minutes, significantly surpassing the efficiencies of CM/O <sub>3</sub> (80%) and titanium alloy/O <sub>3</sub> (70%). After five cycles of catalyst use, the degradation rate of BPA remains at approximately 90%, demonstrating the catalyst's stability.
Fe-Mn/PAC/MB/O <sub>3</sub> <sup>115</sup>	Comparison of the degradation rates of CB/O <sub>3</sub> , MB/O <sub>3</sub> , Fe-Mn/PAC/MB/O <sub>3</sub> on COD and PWW	Ozone concentration 10 mg/L, Fe-Mn/PAC 1 g·L <sup>-1</sup> , reaction time 60 min, pH 7.5-8.5.	Carbon-oxygen functional groups (e.g., C = O, C-OH) and hydroxyl groups on the catalyst surface accelerate ozonolysis and enhance the formation of ·OH and O <sub>2</sub> <sup>·-</sup> . The removals of COD and PWW reached 79% and 95%, respectively. The O <sub>3</sub> decomposition rate was 1.9 times greater than that of MB/O <sub>3</sub> . The exposure to ·OH is ten times greater than that observed with CB/O <sub>3</sub> . The average COD removal efficiency was maintained at around 74% over 100 days of continuous operation with this catalyst, demonstrating good reusability.
Co-CMU/MB/O <sub>3</sub> <sup>116</sup>	Comparison of the degradation rates of CB/O <sub>3</sub> , MB/O <sub>3</sub> , Co-CMU/MB/O <sub>3</sub> on COD	Actual pharmaceutical wastewater, reaction time 45 min, ozone concentration 100 mg/L, Co-CMU 1 g·L <sup>-1</sup> .	Co-CMU is characterized by a high specific surface area and numerous active sites provided by Co <sup>2+</sup> /Co <sup>3+</sup> , enabling the adsorption of ozone and organic pollutants while promoting the production of ·OH and <sup>1</sup> O <sub>2</sub> . The COD removal efficiencies were 20%, 30.7%, and 42.7%, respectively, while the coupled system was 2.5 times less expensive than CB/O <sub>3</sub> . In the five-cycle experiments, the COD removal rates of the Co-CMU catalyst were 50.2%, 49.6%, 45.3%, 46.7%, and 43.7%, respectively. In the first three cycles, the leaching concentrations of Co <sup>2+</sup> were 0.21 mg/L, 0.12 mg/L, and 0.05 mg/L, respectively, confirming the catalyst's good reusability.

The advantages of MNBs in ozone catalytic oxidation technology include an increased residence time of ozone and a high specific surface area that enhances the contact area between pollutants adsorbed on the catalyst and ozone, thereby increasing the reaction rate and ozone utilization. For the same level of ozone depletion, this technology can degrade more pollutants while reducing energy consumption during the reaction. Depending on the nature of the pollutant, adding a small amount of catalyst enables O<sub>3</sub>/MNBs to generate more ·OH, which oxidizes and decomposes organic matter across a wide pH range. This technology reduces the quantities of ozone and catalyst required in actual treatment, thereby lowering process costs. Additionally, this technology aligns with the principles of green environmental protection and can be practically applied as a novel solution for treating organic wastewater.

## 6. Challenges of the coupled system and strategies for green and sustainable development

The coupled system demonstrates high oxidation efficiency and environmental friendliness in real wastewater treatment; however, its application necessitates strict control of multiple risks and process optimization. At the health and safety level, long-term exposure to elevated ozone levels can lead to respiratory irritation, neurotoxicity, and skin damage. In industrial contexts, it can accelerate the aging of rubber and plastic equipment.<sup>117,118</sup> Regarding environmental risks, ozone contributes to the formation of photochemical smog, which exacerbates the greenhouse effect, causes

corrosion of building materials, and inhibits plant photosynthesis.<sup>119</sup> In treating bromine-containing wastewater, bromide ions ( $\text{Br}^-$ ) are oxidized by ozone and  $\cdot\text{OH}$  to form the intermediates  $\text{OBr}^-/\text{HOBr}$ . These intermediates further react with ozone to produce the potent carcinogen bromate ( $\text{BrO}_3^-$ ), which can enter the water column, damaging fish reproductive systems, inhibiting phytoplankton photosynthesis, and infiltrating into the soil.<sup>120</sup> Bromate can damage fish reproductive systems and inhibit phytoplankton photosynthesis upon entering the water, and it can lead to nutrient loss when penetrating the soil. Studies have shown that the  $\text{O}_3/\text{MNBs}$  system exhibits a significantly higher  $\text{BrO}_3^-$  generation rate due to elevated ozone and  $\cdot\text{OH}$  concentrations. The generation of  $\text{BrO}_3^-$  can be inhibited by regulating the reaction pH to below 7 (as  $\text{OBr}^-$  is the main intermediate at  $\text{pH} > 7$ , which accelerates the reaction between  $\text{O}_3$  and  $\text{OBr}^-$  to produce  $\text{BrO}_3^-$ ), selecting a suitable catalyst, or adding  $\text{HCO}_3^-$ .<sup>121,122</sup>

In terms of technology optimization, attention must be given to the secondary hazards posed to ecosystems by intermediates such as aldehydes and ketones, which are produced by the incomplete oxidation of  $\text{O}_3$  and are more toxic than the pollutants themselves.<sup>47</sup> The metal catalyst requires modification to address the ion leaching problem associated with its long-term use. For example, modifying the loading of industrial waste sludge can utilize its porous structure to enhance catalytic efficiency. This can be achieved by coating metal elements to block direct contact with the solution, thereby reducing metal ion leaching and improving catalytic activity under varying water quality conditions. Additionally, this approach supports resource recycling and carbon emission reduction, aligning with the principles of green and sustainable development. Regarding operational specifications, it is recommended to use a closed reactor and configure a real-time ozone concentration monitoring system. Experimental personnel should wear goggles and gas masks, and the tail gas treatment unit should be equipped with an additional  $\text{O}_3$  destructor. Additionally, experimental parameters, such as  $\text{O}_3$  and catalyst dosage, should be optimized based on pollutant characteristics to reduce costs. In industrial wastewater treatment, an ozone concentration detector is employed to monitor ozone levels in real time, ensuring they remain within safe limits and testing whether the treated wastewater meets discharge standards. This system will provide technical support for the green transformation of the wastewater treatment industry through multidimensional risk prevention and control, as well as process innovation.

## 7. Conclusions and outlook

MNBs, characterized by their long residence time, high specific surface area, and interfacial zeta potential, significantly enhance  $\text{O}_3$  dissolution efficiency and mass transfer capacity while increasing the contact area with pollutants. The oxidative degradation of pollutants is enhanced by the release of reactive oxygen species (ROS) such as  $\cdot\text{OH}$  and  $\text{O}_2^{\cdot-}$ , generated through high temperature, pressure, and ionization when the bubbles burst. The efficiency of  $\text{O}_3$  decomposition to generate ROS is further enhanced by combining different types of catalysts. The mechanism involves oxygen vacancies on the catalyst surface, metal redox cycles (e.g.,  $\text{Ce}^{3+}/\text{Ce}^{4+}$ ,  $\text{Fe}^{2+}/\text{Fe}^{3+}$ ), and various synergistic effects such as photocatalytic activity, charge transfer, and chemical bonding. Different loading materials with high chemical inertness, specific surface area, and porosity can further improve catalytic performance and corrosion resistance, reduce metal ion leaching, and enable catalyst recycling. Experiments demonstrated that micro-nano bubbles compensated for the poor  $\text{O}_3$  utilization caused by larger  $\text{O}_3$  bubbles in the ozone catalytic oxidation technique within the coupled system. The rupture of  $\text{O}_3/\text{MNBs}$  across a wide pH range, along with the catalysis of  $\text{O}_3$  using stable novel catalysts, generates large amounts of ROS, demonstrating efficient pollutant degradation under varying pH conditions. This review offers significant theoretical support and technical references for the efficient treatment of organic wastewater.

The coupling of micro-nano bubbles and ozone catalytic oxidation technology overcomes the bottleneck of low efficiency and high energy consumption associated with traditional ozone oxidation. Through the synergistic effects of ROS, it achieves deep mineralization of pollutants while avoiding secondary pollution, aligning with the principles of green sustainable development. However, the current study faces challenges such as insufficient catalyst universality, high energy consumption of MNBs generation equipment, and a lack of industrial validation, necessitating further research.

(1) Future research should focus on designing new multifunctional catalysts. This entails addressing the varying selectivity of different organics to catalysts, the high cost of catalyst production, and catalyst stability. Research should focus on developing new catalysts and membrane materials that are more economical, environmentally friendly,

efficient, and stable, with improved general applicability, oxidative properties, and anti-pollution capabilities.

(2) Optimizing bubble generation equipment through renewable energy sources. The current micro-nano bubble generation equipment faces challenges such as non-uniform bubble size generation and high energy consumption. Future research should focus on improving equipment for bubble size control and consider integrating renewable energy sources, such as solar and wind power, to enhance the sustainability and environmental friendliness of the technology.

(3) Research on scale-up engineering applications. Current ozone-catalyzed oxidation technology is primarily applied in the degradation of organic pollutants. Although micro-nano bubbles enhance the ability of ozone-catalyzed oxidation to degrade pollutants, the combination of these two technologies remains in the laboratory research stage and has not yet been widely implemented in practical industrial operations. In the future, it is essential to conduct continuous actual wastewater tests to optimize and summarize the economic, environmentally friendly, and efficient working mechanisms of the combined technologies based on real data. This will facilitate the transformation of the technology from laboratory settings to industrial applications, providing a more cost-effective and efficient solution for water treatment.

## Acknowledgements

This work was supported by the Scientific Research Fund of Liaoning Provincial Education Department (JYTMS20231216, JYTQN2023285), the Department of Science and Technology of Liaoning Province (2024-BSLH-172), the Shenyang University of Technology (QNPY202209-4), and the Key Laboratory of Functional Inorganic Material Chemistry (Ministry of Education).

## Conflict of interest

The authors declare no conflict of interest.

## References

- [1] Sakr, M.; Mohamed, M. M.; Maraqa, M. A.; Hamouda, M. A.; Aly Hassan, A.; Ali, J.; Jung, J. A critical review of the recent developments in micro-nano bubbles applications for domestic and industrial wastewater treatment. *Alex. Eng. J.* **2022**, *61*(8), 6591-6612.
- [2] Saravanan, A.; Deivayanai, V. C.; Kumar, P. S.; Rangasamy, G.; Hemavathy, R. V.; Harshana, T.; Gayathri, N.; Alagumalai, K. A detailed review on advanced oxidation process in treatment of wastewater: Mechanism, challenges and future outlook. *Chemosphere* **2022**, *308*, 136524.
- [3] Ethiraj, S.; Samuel, M. S.; Indumathi, S. M. A comprehensive review of the challenges and opportunities in microalgae-based wastewater treatment for eliminating organic, inorganic, and emerging pollutants. *Biocatal. Agr. Biotech.* **2024**, *60*, 103316.
- [4] Hu, L.; Xia, Z. Application of ozone micro-nano-bubbles to groundwater remediation. *J. Hazard. Mater.* **2018**, *342*, 446-453.
- [5] Meegoda, J. N.; Aluthgun Hewage, S.; Batagoda, J. H. Stability of nanobubbles. *Environ. Eng. Sci.* **2018**, *35*(11), 1216-1227.
- [6] Zhang, H.; Guo, Z.; Zhang, X. Surface enrichment of ions leads to the stability of bulk nanobubbles. *Soft Matter* **2020**, *16*(23), 5470-5477.
- [7] Kalogerakis, N.; Kalogerakis, G. C.; Botha, Q. P. Environmental applications of nanobubble technology: Field testing at industrial scale. *Can. J. Chem. Eng.* **2021**, *99*(11), 2345-2354.
- [8] Rojviroon, O.; Rojviroon, T. Photocatalytic process augmented with micro/nano bubble aeration for enhanced degradation of synthetic dyes in wastewater. *Water Resour. Ind.* **2022**, *27*, 100169.
- [9] Issaka, E.; Amu-Darko, J. N. O.; Yakubu, S.; Fapohunda, F. O.; Ali, N.; Bilal, M. Advanced catalytic ozonation for degradation of pharmaceutical pollutants-A review. *Chemosphere* **2022**, *289*, 133208.
- [10] Guo, Y.; Long, J.; Huang, J.; Yu, G.; Wang, Y. Can the commonly used quenching method really evaluate the role



of reactive oxygen species in pollutant abatement during catalytic ozonation? *Water Res.* **2022**, *215*, 118275.

- [11] Ma, H.; Chen, G.; Huang, F.; Li, Y.; Zhang, L.; Jin, Y. Catalytic ozonation of ammonia nitrogen removal in wastewater: A review. *J. Water Process. Eng.* **2023**, *52*, 103542.
- [12] Zhang, Z. H.; Wang, S.; Cheng, L.; Ma, H.; Gao, X.; Brennan, C. S.; Yan, J. K. Micro-nano-bubble technology and its applications in food industry: A critical review. *Food Rev. Int.* **2023**, *39*(7), 4213-4235.
- [13] Jin, X.; Wu, C.; Fu, L.; Tian, X.; Wang, P.; Zhou, Y.; Zuo, J. Development, dilemma and potential strategies for the application of nanocatalysts in wastewater catalytic ozonation: A review. *J. Environ. Sci.* **2023**, *124*, 330-349.
- [14] Fan, W.; Li, Y.; Lyu, T.; Yu, J.; Chen, Z.; Jarvis, P.; Huo, Y.; Xiao, D.; Huo, M. A modelling approach to explore the optimum bubble size for micro-nanobubble aeration. *Water Res.* **2023**, *228*, 119360.
- [15] Jin, N.; Zhang, F.; Cui, Y.; Sun, L.; Gao, H.; Pu, Z.; Yang, W. Environment-friendly surface cleaning using micro-nano bubbles. *Particuology* **2022**, *66*, 1-9.
- [16] Lu, J.; Huang, X.; Zhang, Z.; Pang, H.; Chen, K.; Xia, H.; Sui, Y.; Chen, R.; Zhao, Z. Co-coagulation of micro-nano bubbles (MNBs) for enhanced drinking water treatment: A study on the efficiency and mechanism of a novel cleaning process. *Water Res.* **2022**, *226*, 119245.
- [17] Ma, D.; Yin, R.; Liang, Z.; Liang, Q.; Xu, G.; Lian, Q.; Wong, P. K.; He, C.; Xia, D.; Lu, H. Photo-sterilization of groundwater by tellurium and enhancement by micro/nano bubbles. *Water Res.* **2023**, *233*, 119781.
- [18] Wu, M.; Yuan, S.; Song, H.; Li, X. Micro-nano bubbles production using a swirling-type venturi bubble generator. *Chem. Eng. Process.* **2022**, *170*, 108697.
- [19] Xu, W.; Wang, Y.; Huang, Q.; Wang, X.; Zhou, L.; Wang, X.; Wen, B.; Guan, N.; Hu, J.; Zhou, X.; Zhang, L. The generation and stability of bulk nanobubbles by compression-decompression method: The role of dissolved gas. *Colloid. Surface. A.* **2023**, *657*, 130488.
- [20] Zhou, S.; Nazari, S.; Hassanzadeh, A.; Bu, X.; Ni, C.; Peng, Y.; Xie, G.; He, Y. The effect of preparation time and aeration rate on the properties of bulk micro-nanobubble water using hydrodynamic cavitation. *Ultrason. Sonochem.* **2022**, *84*, 105965.
- [21] Mita, M.; Matsushima, H.; Ueda, M.; Ito, H. In-situ high-speed atomic force microscopy observation of dynamic nanobubbles during water electrolysis. *J. Colloid. Interf. Sci.* **2022**, *614*, 389-395.
- [22] Han, S.; Zhu, H. Theoretical and numerical studies on the collapse of single- and double-bubble system in water. *Int. J. Numer. Meth. Fl.* **2021**, *93*(3), 527-542.
- [23] Zhang, H.; Xue, X.; Lin, S.; Zhang, Z.; Wu, N.; Yang, W.; Ren, Q.; Zhao, Y. Micro-nano bubble generating technology and its application in hydroponics with aeration. *Vegetables* **2019**, *1*, 59-65.
- [24] Atkinson, A. J.; Apul, O. G.; Schneider, O.; Garcia-Segura, S.; Westerhoff, P. Nanobubble technologies offer opportunities to improve water treatment. *Acc. Chem. Res.* **2019**, *52*(5), 1196-1205.
- [25] Zhang, F.; Li, S.; Liu, T.; Zhang, P.; Wang, B.; Li, X. Application of nanobubble technique on soil-crop system: A review. *Chin. J. Ecol.* **2024**, 1-10.
- [26] Soyluoglu, M.; Kim, D.; Zaker, Y.; Karanfil, T. Stability of oxygen nanobubbles under freshwater conditions. *Water. Res.* **2021**, *206*, 117749.
- [27] Fan, W.; Zhou, Z.; Wang, W.; Huo, M.; Zhang, L.; Zhu, S.; Yang, W.; Wang, X. Environmentally friendly approach for advanced treatment of municipal secondary effluent by integration of micro-nano bubbles and photocatalysis. *J. Clean. Prod.* **2019**, *237*, 117828.
- [28] Sun, L.; Zhang, F.; Yang, W. Research progress of hydroxyl radicals formed by micro-nanobubble. *Water. Purif. Technol.* **2021**, *40*(2), 37-41.
- [29] Thi Phan, K. K.; Truong, T.; Wang, Y.; Bhandari, B. Nanobubbles: Fundamental characteristics and applications in food processing. *Trends Food Sci. Tech.* **2020**, *95*, 118-130.
- [30] Lyu, T.; Wu, S.; Mortimer, R. J. G.; Pan, G. Nanobubble technology in environmental engineering: Revolutionization potential and challenges. *Environ. Sci. Technol.* **2019**, *53*(13), 7175-7176.
- [31] Yang, J.; Zhang, R.; Chen, L.; Li, Q.; Zhang, Z.; Sun, X. Research progress on pollutant degradation by micro-nano bubbles composite advanced oxidation technology. *Technol. Water Treat.* **2022**, *48*(3), 25-29.
- [32] Hewage, S. A.; Kewalramani, J.; Meegoda, J. N. Stability of nanobubbles in different salts solutions. *Colloid Surf. A.* **2021**, *609*, 125669.
- [33] Levitsky, I.; Tavor, D.; Gitis, V. Micro and nanobubbles in water and wastewater treatment: A state-of-the-Art review. *J. Water Process. Eng.* **2022**, *47*, 102688.
- [34] Temesgen, T.; Bui, T. T.; Han, M.; Kim, T.; Park, H. Micro and nanobubble technologies as a new horizon for water-treatment techniques: A review. *Adv. Colloid Interface Sci.* **2017**, *246*, 40-51.
- [35] Aluthgun Hewage, S.; Batagoda, J. H.; Meegoda, J. N. In situ remediation of sediments contaminated with organic

- pollutants using ultrasound and ozone nanobubbles. *Environ. Eng. Sci.* **2020**, *37*(8), 521-534.
- [36] Li Z.; Liao G.; Zhan, X. Study on characterization of micron-nano bubbles. *Guangzhou Chem. Ind.* **2022**, *50*(22), 53-55.
- [37] Michailidi, E. D.; Bomis, G.; Varoutoglou, A.; Kyzas, G. Z.; Mitrikas, G.; Mitropoulos, A. Ch.; Efthimiadou, E. K.; Favvas, E. P. Bulk nanobubbles: Production and investigation of their formation/stability mechanism. *J. Colloid Interface Sci.* **2020**, *564*, 371-380.
- [38] Wang, Q.; Zhao, H.; Qi, N.; Qin, Y.; Zhang, X.; Li, Y. Generation and stability of size-adjustable bulk nanobubbles based on periodic pressure change. *Sci. Rep.* **2019**, *9*(1), 1118.
- [39] Du, M.; Wang, Y.; Gao, Q.; Zhang, Y.; Sun, X. Mechanism and efficiency of ozone microbubble treatment of organic wastewater. *Chem. Ind. Eng. Prog.* **2021**, *40*(12), 6907-6915.
- [40] Yasuda, K.; Matsushima, H.; Asakura, Y. Generation and reduction of bulk nanobubbles by ultrasonic irradiation. *Chem. Eng. Sci.* **2019**, *195*, 455-461.
- [41] Lee, J. I.; Kim, J. M. Influence of temperature on bulk nanobubble generation by ultrasonication. *Colloid. Interfac. Sci.* **2022**, *49*, 100639.
- [42] Zhu, J.; An, H.; Alheshibri, M.; Liu, L.; Terpstra, P. M. J.; Liu, G.; Craig, V. S. J. Cleaning with bulk nanobubbles. *Langmuir* **2016**, *32*(43), 11203-11211.
- [43] Li, X.; Fu, L.; Chen, F.; Zhao, S.; Zhu, J.; Yin, C. Application of heterogeneous catalytic ozonation in wastewater treatment: An overview. *Catalysts* **2023**, *13*(2), 342.
- [44] Jin, X.; Zhang, S.; Yang, S.; Zong, Y.; Xu, L.; Jin, P.; Yang, C.; Hu, S.; Li, Y.; Shi, X.; Wang, X. C. Behaviour of ozone in the hybrid ozonation-coagulation (HOC) process for ibuprofen removal: Reaction selectivity and effects on coagulant hydrolysis. *Sci. Total Environ.* **2021**, *794*, 148685.
- [45] Jin, S.; Lv, R. Research progress of heterogeneous catalytic ozonation for industrial wastewater treatment. *Inorg. Chem. Ind.* **2024**, *56*(3), 28-38.
- [46] Wang, H.; Yu, X.; Yue, L.; Chen, Y.; Chen, G.; Xu, H.; Shi, H.; Sun, X. The technical study of ozone catalytic oxidation for nanofiltration concentrated liquid of kitchen and food waste digestate. *Shandong Chem. Ind.* **2023**, *52*(20), 264-269.
- [47] Mahmoodi, M.; Pishbin, E. Ozone-based advanced oxidation processes in water treatment: Recent advances, challenges, and perspective. *Environ. Sci. Pollut. Res.* **2025**, *32*(7), 3531-3570.
- [48] Ochiai, T.; Hamada, K.; Okui, M. Synergistic effects of photocatalysis, ozone treatment, and metal catalysts on the decomposition of acetaldehyde. *Catalysts* **2025**, *15*(2), 141.
- [49] Cao, S.; Chen, L.; Zhao, M.; Liu, A.; Wang, M.; Sun, Y. Advanced treatment of phosphorus pesticide wastewater using an integrated process of coagulation and ozone catalytic oxidation. *Catalysts* **2022**, *12*(1), 103.
- [50] Xiang, Y.; Jiang, H.; Wei, H.; Liu, X.; Zou, P. Research and application of heterogeneous catalytic ozonation in advanced treatment for refractory organic wastewater of biochemical tailwater. *Water Purif. Technol.* **2023**, *42*(1), 40-50.
- [51] Zhu, M.; Yuan, S.; Liu, J.; Pan, S.; Zhou, H. Research progress on treatment of organic wastewater using heterogeneous ozone catalytic oxidation technology. *Chem. Reagents* **2024**, *46*(3), 1-7.
- [52] Shen, D.; Xie, Z.; Shentu, J.; Long, Y.; Lu, L.; Li, L.; Qi, S. Enhanced oxidation of aromatic hydrocarbons by ozone micro-nano bubble water: Mechanism and influencing factors. *J. Environ. Chem. Eng.* **2023**, *11*(3), 110281.
- [53] Li, R.; Hong, M.; Guo, M.; Chen, R.; Song, B. Oxidation and degradation of nitrobenzene by ozone micro-nano bubbles. *Chem. Eng. Sci.* **2025**, *302*, 120903.
- [54] Chen, H. L.; Arcega, R. D.; Liao, P. Y.; Hou, C. Y.; Liu, W. C.; Chen, Y. R.; Wu, J. S.; Wang, W. R.; Lin, C. M. Reduction of pesticides and bacteria on napa cabbage by ozone microbubble water. *Postharvest Biol. Technol.* **2023**, *204*, 112444.
- [55] Zhang, J.; Lv, S.; Yu, Q.; Liu, C.; Ma, J.; Jia, M.; Fang, S. Degradation of sulfamethoxazole in microbubble ozonation process: Performance, reaction mechanism and toxicity assessment. *Sep. Purif. Technol.* **2023**, *311*, 123262.
- [56] Kizhisseri, M. I.; Sakr, M.; Maraqa, M.; Mohamed, M. M. A comparative bench scale study of oxygen transfer dynamics using micro-nano bubbles and conventional aeration in water treatment systems. *Heliyon* **2025**, *11*(4), e41687.
- [57] Zhang, Q.; Wang, X.; Wu, N.; Zhu, C.; Qin, W.; Huang, D.; Zhou, D. Advanced reduction processes initiated by oxidative radicals for trichloroacetic acid degradation: Performance, radical generation, and mechanism. *Water Res.* **2025**, *268*, 122587.
- [58] Hu, L.; Cao, Y.; Xia, Z.; Lin, D. Physical modeling of organics-contaminated groundwater remediation by ozone

- micro-nano-bubbles enhanced oxidation. *J. Hydrol.* **2024**, *645*, 132176.
- [59] Hu, L.; Chen, B.; Ma, J. Micro-/nano- bubbles ozonation for effective industrial wastewater remediation: From lab to pilot-scale application. *J. Environ. Chem. Eng.* **2023**, *11*(5), 110807.
- [60] Sun, C.; Wang, Y.; Jiang, B.; Hu, S.; Wang, Y.; Zhang, C.; Liu, F.; Zhang, Y.; Li, G. Self-catalyst degradation of amoxicillin in alkaline condition driven by superoxide radical. *Chem. Eng. J.* **2023**, *477*, 146942.
- [61] Dai, M.; Niu, Q.; Wu, S.; Lin, Y.; Biswas, J. K.; Yang, C. Hydroxyl radicals in ozone-based advanced oxidation of organic contaminants: A review. *Environ. Chem. Lett.* **2024**, *22*(6), 3059-3106.
- [62] Xu, S. L.; Wang, W.; Song, Y.; Tang, R.; Hu, Z. H.; Zhou, X.; Yu, H. Q. Expanding the pH range of Fenton-like reactions for pollutant degradation: the impact of acidic microenvironments. *Water Res.* **2025**, *270*, 122851.
- [63] Ma, Y.; An, Z.; Li, M.; Huo, Y.; Zhou, Y.; Jiang, J.; He, M. Theoretical study on the degradation mechanisms, degradation efficiencies, and toxicity evaluation of 2-chlorophenylacetonitrile by hydroxyl radical in the aqueous phase. *J. Mol. Liq.* **2025**, *417*, 126617.
- [64] Zhang, L.; Li, P.; Wang, X.; He, X.; Li, E.; Lan, Q.; Liu, Y.; Yin, D. Promotion effect of foam formation on the degradation of polyvinyl alcohol by ozone microbubble. *J. Environ. Chem. Eng.* **2023**, *11*(6), 111192.
- [65] Zhang, J.; Liu, M.; Pang, B.; Liu, C.; Ma, J.; Niu, J.; Zhang, R. Ciprofloxacin degradation in microbubble ozonation combined with electro-generated  $H_2O_2$  process: Operational parameters and oxidation mechanism. *Sep. Purif. Technol.* **2023**, *325*, 124676.
- [66] Jiang, M.; Guo, R.; Guo, C.; Xu, J. Efficiency and mechanism of oxidative degradation of typical UV filters by ozone micro-nano bubbles. *J. Environ. Chem. Eng.* **2024**, *14*(1), 1121-1129.
- [67] Che, S.; Jia, Y.; Li, Y. Design and synthesis of self-supported water-splitting transition metal-based electrocatalysts via electrospinning. *Catalysts* **2025**, *15*(3), 205.
- [68] Ziwei, Y.; Zhe, W.; Shaopo, W.; Jingjie, Y.; Chen, L.; Jing, C. Mechanism of ozone catalysis by transition metal hydroxyl oxides: From reactive oxygen species to surface structural hydroxyl. *Desalin. Water Treat.* **2024**, *320*, 100823.
- [69] Ma, H.; Li, W.; Liu, B.; Hu, H.; Li, Y.; Xu, W.; Fang, R.; Dong, F. Oxygen vacancies induced intrinsic electric field attenuation for superior molecular oxygen activation and NO oxidation. *Chem. Eng. J.* **2025**, *505*, 159421.
- [70] Luo, D.; Luo, R.; Wang, X.; Chang, X.; Yang, T.; Chen, S.; Zhao, Z. J.; Gong, J. Role and regulation of surface oxygen vacancies in vanadium-based oxides for chemical looping oxidative dehydrogenation of propane. *Chem. Sci.* **2025**, *16*, 4710-4717.
- [71] Chen, W.; He, H.; Liang, J.; Wei, X.; Li, X.; Wang, J.; Li, L. A comprehensive review on metal based active sites and their interaction with  $O_3$  during heterogeneous catalytic ozonation process: Types, regulation and authentication. *J. Hazard. Mater.* **2023**, *443*, 130302.
- [72] Flores Alberto, E.; Rodríguez Santillán, J. L.; Poznyak, T.; De la Cruz Salazar, I. J.; Sánchez Vargas, D.; Fuentes Camargo, I.; Guzmán Castañeda, J. I. Sequential ozonation processes for enhanced degradation of aromatic sulfonic compounds in water. *Water Air Soil Poll.* **2025**, *236*(2), 100.
- [73] Zhou, B.; Zhang, X.; Wang, P.; Zhang, X.; Wei, C.; Wang, Y.; Wen, G. Catalytic performance and insight into the mechanism of  $CeO_2$  nanorod catalysts in phenol ozone oxidation reaction. *Ceram. Int.* **2024**, *50*(1), 394-402.
- [74] Majhool, A. K.; Sukkar, K. A.; Alsaffar, M. A.; Majdi, H. S. Integrated process for high phenol removal from wastewater employing a zno nanocatalyst in an ozonation reaction in a packed bubble column reactor. *Chem Eng.* **2023**, *7*(6), 112.
- [75] Liao, G.; Qing, X.; Lai, X.; Liang, Z.; Jiang, S.; Xie, Z.; Fang, J.; Lan, B.; Chen, W.; Wang, J.; Li, L. Efficient treatment of surfactant containing wastewater by photocatalytic ozonation with  $BiPO_4$  nanorods. *Chemosphere* **2024**, *346*, 140594.
- [76] Chen, Y.; Chen, R.; Chang, X.; Yan, J.; Gu, Y.; Xi, S.; Sun, P.; Dong, X. Ozone catalysis degradation of sodium acetate via vacancy-driven radical oxidation over Fe-modified fly ash. *Water* **2023**, *15*(21), 3801.
- [77] Chen, S.; Ren, T.; Zhou, Z.; Lu, K.; Huang, X.; Zhang, X. Insights into Mn loaded carbon-silica-membrane based catalytic ozonation process for efficient wastewater treatment: Performance and mechanism. *Chem. Eng. J.* **2023**, *475*, 145874.
- [78] Wang, A.; Wu, Y.; Shen, X.; Zhang, Q.; Jian, H.; Han, C. Efficient ozone decomposition by amorphous Mn-Ni bimetallic catalysts under an entire humidity environment. *J. Environ. Chem. Eng.* **2024**, *12*(5), 113848.
- [79] Zhong, J.; Mao, X.; Wang, G.; Li, H.; Li, J.; Qu, S.; Zhao, J. Synthesis of Cu/Mn/Ce polymetallic oxide catalysts and catalytic ozone treatment of wastewater. *RSC Adv.* **2024**, *14*(48), 35993-36004.
- [80] Li, X.; Wang, Z.; Qin, X.; Zhang, F.; Xu, C.; Tao, X.; Ren, H.; Lan, X. Enhancing Fenton-like degradation efficiency over a broad pH range through synergistic interactions among varied acidity sites in  $M_1-O-M_2$  structures.

*Sep. Purif. Technol.* **2025**, 353, 128366.

- [81] Chen, W.; He, H.; Zou, R.; Chen, Y.; Li, X.; Wang, J.; Tang, Y.; Li, L. Unravelling the facets-dependent behavior among H<sub>2</sub>O<sub>2</sub>, O<sub>3</sub> and Oxygen vacancies on CeOx and the promotion of peroxone reaction at under acidic conditions. *Environ. Sci-Nano.* **2021**, 8(11), 3138-3152.
- [82] Liang, Y.; Zhang, Z.; Su, X.; Feng, X.; Xing, S.; Liu, W.; Huang, R.; Liu, Y. Coordination defect-induced frustrated lewis pairs in polyoxo-metalate-based metal-organic frameworks for efficient catalytic hydrogenation. *Angewandte Chemie* **2023**, 135(37), e202309030.
- [83] Sun, W.; Xiao, Z.; Sun, Y.; Ding, L.; Zhou, J. Preparation of Cu-Ce@ $\gamma$ -Al<sub>2</sub>O<sub>3</sub> and study on catalytic ozone oxidation for the treatment of RO concentrate water. *Water* **2022**, 14(18), 2881.
- [84] Bai, H.; Liang, L.; Cao, P.; Zhang, H.; Chen, S.; Yu, H.; Quan, X. Micro-nanobubble-ozone catalytic oxidation to remove organic matter from uranium purification wastewater. *Appl. Catal. B-Environ.* **2024**, 343, 123527.
- [85] Yan, Z.; Zhu, J.; Hua, X.; Liang, D.; Dong, D.; Guo, Z.; Zheng, N.; Zhang, L. Catalytic ozonation for the degradation of polyvinyl alcohol in aqueous solution using catalyst based on copper and manganese. *J. Clean. Prod.* **2020**, 272, 122856.
- [86] Chen, Y.; Liu, D.; Chen, Q.; Long, Y.; Wang, C.; Wu, W. Study on the FeCu-C@MS catalytic ozonation for the degradation of cumene hydroperoxide wastewater. *Technol. Water Treat.* **2024**, 50(2), 57-61.
- [87] Feng, J.; Xing, B.; Chen, H. Catalytic ozonation of humic acid in water with modified activated carbon: Enhancement and restoration of the activity of an activated carbon catalyst. *J. Environ. Manage.* **2019**, 237, 114-118.
- [88] Zhou, B.; Chen, X.; Li, M.; Zhang, J.; Sun, J. Experimental study on the catalytic ozonation degradation of oxalic acid by ammonia hydrothermal modified activated carbon fibers. *J. Zhejiang Agric. Sci.* **2023**, 64(4), 949-953.
- [89] Jia, W.; Li, Y.; Chen, C.; Wu, Y.; Liang, Y.; Du, J.; Feng, X.; Wang, H.; Wu, Q.; Guo, W. Q. Unveiling the fate of metal leaching in bimetal-catalyzed fenton-like systems: Pivotal role of aqueous matrices and machine learning prediction. *J. Hazard. Mater.* **2024**, 477, 135291.
- [90] Özçakır, G.; Açıkgöz, Ç. Unveiling activity of zif-8/nickel loaded alumina aerogel catalyst in glycerol carbonate production from CO<sub>2</sub> and glycerol. *Res. Chem. Intermediat.* **2024**, 50(12), 5655-5678.
- [91] Jiang, X.; Guan, S.; Chen, L.; Deng, F.; Yan, H.; Liu, F.; Zhai, X.; Martínez-Huitle, C. A.; Ding, J. Designing carbon-based catalysts for enhanced sulfite activation: Strategies for pollutant degradation. *J. Environ. Chem. Eng.* **2024**, 12(6), 114719.
- [92] Zou, Q.; Wang, B.; Gao, B.; Jiang, T.; Feng, Q.; Chen, M.; Zhang, J.; Zhang, X. Roles and mechanisms of carbonaceous materials in advanced oxidation coupling processes for degradation organic pollutants in wastewater: A review. *Biochar* **2023**, 5(1), 86.
- [93] Wang, H.; Xu, Z.; Yang, X. Probing the formation mechanisms of reactive oxygen species in graphene oxide-catalyzed ozone advanced oxidation processes. *Carbon* **2025**, 233, 119831.
- [94] Teng, X.; Si, D.; Chen, L.; Shi, J. Synergetic catalytic effects by strong metal-support interaction for efficient electrocatalysis. *eScience* **2024**, 4(6), 100272.
- [95] Wang, H.; Gao, Z.; Sun, B.; Mu, S.; Dang, F.; Guo, X.; Ma, D.; Shi, C. Engineering metal-support interaction to construct catalytic interfaces and redisperse metal nanoparticles. *Chem. Catalysis* **2023**, 3(10), 100768.
- [96] Guo, J.; Yao, Y.; Yan, X.; Meng, X.; Wang, Q.; Zhang, Y.; Yan, S.; Zhao, X.; Luo, S. Emerging carbon-based catalysts for the oxygen reduction reaction: Insights into mechanisms and applications. *Inorganics* **2024**, 12(12), 303.
- [97] Lee, W.; Kwon, S. Role of acid treatment of the carbon support in the growth of atomic-layer-deposited Pt nanoparticles for PEMFC fabrication. *Part. Part. Syst. Char.* **2023**, 40(2), 2200158.
- [98] Wang, J.; Fu, L.; Chen, X.; Deng, L.; Wu, C. Catalytic ozonation promoted by mn-doped sludge-based catalyst treating refractory industrial wastewater. *Sep. Purif. Technol.* **2025**, 354, 128676.
- [99] Yadav, S.; Mittal, A.; Sharma, S.; Sharma, A.; Kumari, K.; Kumar, N. Highly efficient Ag<sub>2</sub>O loaded ZnO/Al<sub>2</sub>O<sub>3</sub> coupled catalyst and its photocatalytic application. *Inorg. Chem. Commun.* **2021**, 130, 108738.
- [100] Oliveira, G. V.; de Macedo, V.; Urquiza-González, E. A.; Magriotis, Z. M.; Pereira, C. A. Fe<sub>2</sub>O<sub>3</sub>/ $\gamma$ -Al<sub>2</sub>O<sub>3</sub> and NiO/ $\gamma$ -Al<sub>2</sub>O<sub>3</sub> catalysts for the selective catalytic oxidation of ammonia. *Catal. Today* **2025**, 444, 114991.
- [101] Kwak, J. H.; Hu, J.; Mei, D.; Yi, C. W.; Kim, D. H.; Peden, C. H. F.; Allard, L. F.; Szanyi, J. Coordinatively unsaturated Al<sup>3+</sup> centers as binding sites for active catalyst phases of platinum on  $\gamma$ -Al<sub>2</sub>O<sub>3</sub>. *Science* **2009**, 325(5948), 1670-1673.
- [102] Zhao, Z.; Xiao, D.; Chen, K.; Wang, R.; Liang, L.; Liu, Z.; Hung, I.; Gan, Z.; Hou, G. Nature of five-coordinated Al in  $\gamma$ -Al<sub>2</sub>O<sub>3</sub> revealed by ultra-high-field solid-state NMR. *ACS Cent. Sci.* **2022**, 8(6), 795-803.



- [103] Fatehi Haghighat, M.; Mortazavi-Manesh, A.; Hashemi Dehkordi, S. A.; Goshtasbi Hassanabadi, P.; Bahadoran, F.; Safari, N. Synthesis of  $\gamma$ - $\text{Al}_2\text{O}_3$ - $\text{CeO}_2$  catalyst with high surface area, high stability, and less coke formation for methanol dehydration reaction process. *J. Iran. Chem. Soc.* **2024**, *21*(4), 903-912.
- [104] Zhang, C.; Liu, F.; Mu, Y.; Wu, M.; Lin, Y.; Wang, S.; Liu, H.; Cheng, P.; Xu, K.; Han, G. High-strength, high-porosity and low-shrinkage  $\text{Al}_2\text{O}_3$  ceramics prepared by flexible adjustment of  $\text{CaCO}_3$  size and content. *J. Eur. Ceram. Soc.* **2024**, *44*(4), 2304-2316.
- [105] Zhang, Z.; Du, C.; Li, H.; Hu, J.; Yang, F.; Huang, J.; Hu, S.; Li, W.-X.; Xiong, H. Spatial segregation of three-dimensional  $\text{Al}_2\text{O}_3$  supported PtSn catalyst for improved sintering-resistant at high temperature. *Appl. Catal. B-Environ.* **2024**, *358*, 124334.
- [106] Geng, L.; Zhang, X.; Wang, X. Micro-nanobubble-ozone catalytic oxidation to remove organic matter from uranium purification wastewater. *China Nucl. Power* **2023**, *16*(4), 562-567.
- [107] Wei, J.; Zhu, Y.; Wang, S.; Wang, R. Influencing factors of dye wastewater by catalytic oxidation with Mn/GAC-Ozone micro-nano bubbles. *J. Civ. Environ. Eng.* **2025**, *47*(2), 232-240.
- [108] Wang, S.; Wang, Y.; Meng, F.; Li, W.; You, H. Degradation of quinoline and its mechanism by catalytic ozonation with  $\text{MnO}_2/\text{Al}_2\text{O}_3$  catalyst. *Acta Sci. Circumstantiae.* **2020**, *40*(10), 3651-3657.
- [109] Zhu, X.; Wang, B.; Kang, J.; Shen, J.; Yan, P.; Li, X.; Yuan, L.; Zhao, S.; Cheng, Y.; Li, Y.; Zuo, J.; Chen, Z. Interfacial mechanism of the synergy of biochar adsorption and catalytic ozone micro-nano-bubbles for the removal of 2,4-dichlorophenoxyacetic acid in water. *Sep. Purif. Technol.* **2022**, *299*, 121777.
- [111] Wei, J.; Sha, H.; Wang, R. Study on treatment of basic yellow 28 dye wastewater by micro-nano bubble ozone catalytic oxidation. *Environ. Eng. Res.* **2023**, *28*(5), 220606.
- [112] Zhang, J.; Yang, L.; Liu, C.; Ma, J.; Yan, C.; Mu, S.; Yu, M. Efficient degradation of tetracycline hydrochloride wastewater by microbubble catalytic ozonation with sludge biochar-loaded layered polymetallic hydroxide. *Sep. Purif. Technol.* **2024**, *340*, 126767.
- [113] Zeng, K.; Liu, Y.; Lin, D.; Chen, W.; Huang, C.; Chen, J. Advanced treatment of papermaking wastewater by combined process of  $\gamma$ - $\text{FeOOH}$  catalyzed ozone microbubble and BAF. *Water Purif. Technol.* **2023**, *42*(2), 117-124.
- [113] Zhang, J.; Yang, X.; Kang, F.; Liu, C.; Lv, S.; Liu, M.; Pang, B. Performance of advanced treatment of pharmaceutical wastewater by microbubble catalytic ozonation and component variation characteristics of dissolved organic matter. *Chin. J. Environ. Eng.* **2022**, *16*(5), 1469-1479.
- [114] Zhang, E.; Xu, G.; Wang, H.; Jin, S.; Wang, X.; Liu, L.; Tian, J. Ultra-high efficient catalytic degradation of BPA by ozone-function microbubble aerated ceramic membrane for water purification. *Ceram. Int.* **2024**, *50*(24), 54447-54457.
- [115] Jothinathan, L.; Cai, Q. Q.; Ong, S. L.; Hu, J. Y. Fe-Mn doped powdered activated carbon pellet as ozone catalyst for cost-effective phenolic wastewater treatment: Mechanism studies and phenol by-products elimination. *J. Hazard. Mater.* **2022**, *424*, 127483.
- [116] Wang, S.; Qiu, J.; Ren, M.; Cui, Y.; Xie, Y.; Cao, H. Enhanced treatment of reverse osmosis concentrates by ozone micro-nano bubbles coupled with catalytic ceramic membranes. *J. Water Process Eng.* **2024**, *61*, 105213.
- [117] Wang, Y.; Yang, Y.; Yuan, Q.; Li, T.; Zhou, Y.; Zong, L.; Wang, M.; Xie, Z.; Ho, H. C.; Gao, M.; Tong, S.; Lolli, S.; Zhang, L. Substantially underestimated global health risks of current ozone pollution. *Nat. Commun.* **2025**, *16*(1), 102.
- [118] Treib, C.; Loos, K.; Johlitz, M.; Lion, A. Ozone ageing: Experimental methods on pristine and protected natural rubber. *Continuum Mech. Thermodyn.* **2022**, *34*(6), 1563-1577.
- [119] Wang, Z.; Zhang, H.; Shi, C.; Ji, X.; Zhu, Y.; Xia, C.; Sun, X.; Zhang, M.; Lin, X.; Yan, S.; Zhou, Y.; Xing, C.; Chen, Y.; Liu, C. Vertical and spatial differences in ozone formation sensitivities under different ozone pollution levels in eastern Chinese cities. *npj Clim. Atmos. Sci.* **2025**, *8*(1), 1-14.
- [120] Wen, G.; Qiang, C.; Feng, Y.; Huang, T.; Ma, J. Bromate formation during the oxidation of bromide-containing water by ozone/peroxymonosulfate process: Influencing factors and mechanisms. *Chem. Eng. J.* **2018**, *352*, 316-324.
- [121] Zuo, J.; Xu, X.; Wan, Q.; Cao, R.; Liang, Z.; Xu, H.; Li, K.; Huang, T.; Wen, G.; Ma, J. Inactivation of fungal spores in water with peracetic acid: Efficiency and mechanism. *Chem. Eng. J.* **2022**, *427*, 131753.
- [122] Wang, J.; Wang, S. Effect of inorganic anions on the performance of advanced oxidation processes for degradation of organic contaminants. *Chem. Eng. J.* **2021**, *411*, 128392.